Triphenylamine and some of its derivatives as versatile building blocks for organic electronic applications

Philippe Blanchard, Claudia Malacrida, Clément Cabanetos, Jean Roncali, Sabine Ludwigs

Triphenylamine and some of its derivatives as versatile building blocks for organic electronic applications

Philippe Blanchard,*[a] Claudia Malacrida,[b] Clément Cabanetos,[a] Jean Roncali[a] and Sabine Ludwigs*[b]

[a] Group Linear Conjugated Systems, MOLTECH-Anjou, CNRS UMR 6200, University of Angers, 2 Bd Lavoisier, 49045 Angers, France

[b] IPOC - Functional Polymers, Institute of Polymer Chemistry, University of Stuttgart, Pfaffenwaldring 55, 70569 Stuttgart, Germany

Corresponding authors: philippe.blanchard@univ-angers.fr; sabine.ludwigs@ipoc.uni-stuttgart.de

Keywords – triphenylamine, electrochemistry, crosslinking, push-pull molecules, organic solar cells, polymers

Abstract:

This review article gives an overview of past and current activities in the *Linear Conjugated Systems* group of Angers and in the *IPOC - Functional Polymers* group of the Institute of Polymer Chemistry of Stuttgart on the use of triphenylamine (TPA) as versatile building block for organic electronics. In the first part, the properties of TPA itself are introduced including geometrical and energy level considerations. Dimerization of TPA to tetraphenylbenzidine (TPB) upon electrochemical oxidation is highlighted. The blocking of TPA *para*-positions and its implications in terms of electroactivity is further discussed. The second part shows that dimerization of TPA as pendant redox-active moieties in polymers is a versatile strategy to crosslink polymer films. Coming from redox homopolymers the crosslinking strategy is extended towards conjugated redox polymers based on polythiophenes and block copolymers. Conductivity mechanisms and the influence of doping level on conductivity is probed with cyclic voltammetry coupled with in-situ conductance and four point probe measurements. The last part is dedicated to the use of TPA as electron-donating block in the design of donor-π-acceptor chromophores and their use as active material in organic photovoltaics. An overview of some relevant TPA-based push-pull molecules from literature and our contribution to this field are presented emphasizing the progress of the photovoltaic performances of organic solar cells made over the last decade.

Introduction

Triphenylamine (TPA) derivatives are a class of versatile redox active molecules that have attracted particular attention in relation to their promising hole transport properties.[1–4] Applications include various thin layer opto-electronic devices[1,5,6] comprising organic light emitting diodes (OLEDs),[7,8] electrochromic devices,[9] dye sensitized solar cells, organic solar cells (OSCs)[10–12] and perovskite solar cells.[12–14] The electron-rich character of TPA has also been exploited for electrochemical storage of energy[15] and electrical memory devices.[16,17] The use of TPA derivatives is particularly appealable due to a number of desirable properties, including their synthetic accessibility and the possibility of finely tuning their redox and absorption characteristics.

After an introduction on the structural and electronic properties of TPA, this review article will discuss, through some examples, the interest of TPA to trigger chemical or electrochemical couplings affording cross-linked electroactive and nanostructured polymer films. Then, an overview of push-pull molecules derived from TPA will be presented showing the interest of this major class of compounds as donor materials for organic photovoltaics (OPV) and the considerable progress achieved over the last decade.

In this context, the past and current research activities of our groups devoted to these fields will be emphasized.

Structural and electronic properties of TPA

TPA is a tertiary amine bearing three aromatic groups. Because of the resonance delocalization of the electron lone pair on its entire molecular structure, TPA is characterized by a very low basicity compared to aliphatic amines.

Different synthetic ways for TPA-type molecules are known. They can for example be obtained by modifications of the Ullmann condensation reaction (1903) through the nucleophilic substitution of an aryl-halide in the presence of a copper catalyst and a base.[18,19] More recently, the use of palladium catalysts with phosphine ligands was found to be a successful approach for the synthesis of TPA derivatives such as mixed secondary arylamines obtained from amination of aryl halides,[20,21] allowing milder reaction conditions and easier separation and crystallization steps. For example, among several phosphine ligated palladium complexes, Buchwald *et al*. proposed the use of a catalytic system constituted of BINAP (2,2'-bis(diphenylphosphino)-1,1'-binaphthyl) and $Pd_2(dba)_3$.[21] Iron-catalyzed aromatic amination for synthesizing diaryl- and triarylamines has also been successfully developed.[22]

The molecular geometry of TPA results from two opposing factors: the resonance stabilization of the π-electron systems and the steric repulsion of protons of neighboring phenyl rings (Figure 1b).[4] A planar geometry (D3h symmetry) is favored to maximize the conjugation of the π-electron systems of the phenyl groups, on the other hand the steric repulsions are minimized through their tilting from the plane. These two factors lead to a propeller like structure (C3 symmetry). X-ray measurements and computational calculations agree for an average C−N bond length of 1.42 Å, a C−N−C bond angle of 120°, and an optimum tilting of phenyl groups through a torsional angle of 42° with respect to the CCCN plane.[4,23–25]

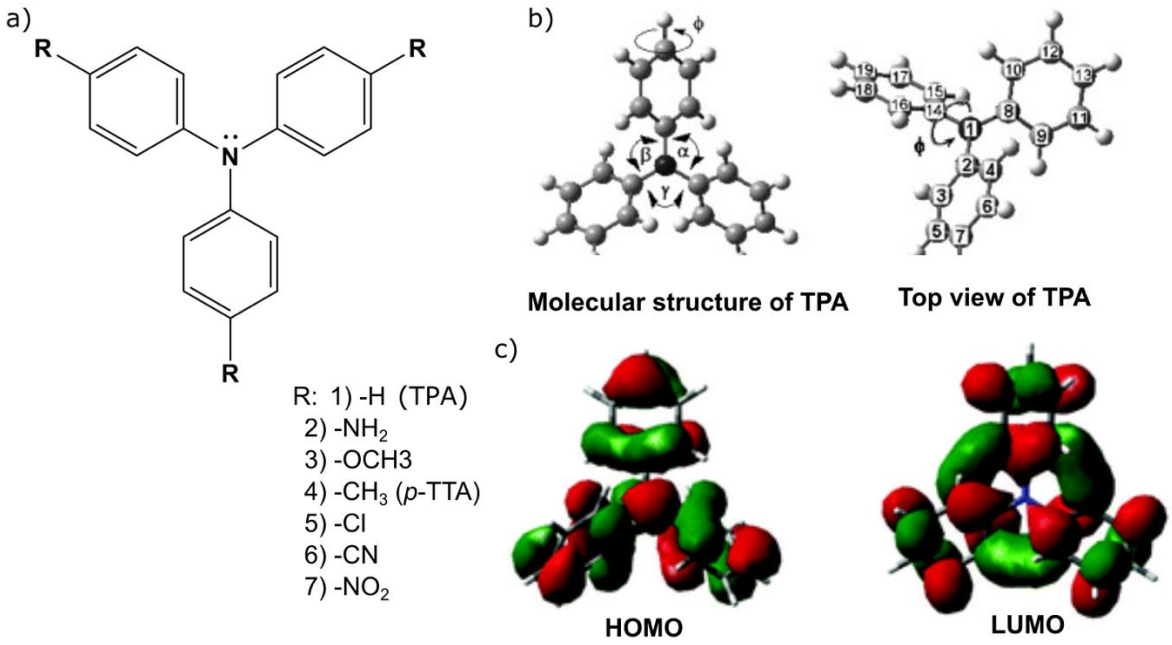

Figure 1: a) Chemical structures of TPA and *para*-substituted derivatives. **b)** Propeller like structure of TPA with three tilted phenyl rings. Adapted from ref. 25. **c)** DFT calculated HOMO and LUMO for TPA. Figure adapted from ref. 4.

Figure 1c shows DFT calculations of the frontier molecular orbitals of TPA. The HOMO of TPA is delocalized over the whole molecule, with highest amplitude of the energy density over the phenyl rings and the p-orbital of the central nitrogen. In the case of the LUMO no contribution of the central nitrogen is observed.

The molecule oxidation and therefore removal of an electron from the HOMO causes a limited change of the electron density on the nitrogen, and *ortho, meta*, *para* position on phenyl rings.[23]

According to Gescheidt *et al*. the calculated ionization potential (I_p) of TPA is 6.608 eV; it is index of the good electron-donating capability of the molecule.[4] Calculated HOMO and LUMO levels for TPA are -5.188 eV and -0.720 eV, respectively.[4] The effects of substituents (Figure 1a) on HOMO-LUMO levels, ionization potentials and on the molecular geometry of TPA have been widely investigated through the years.[4,26–28]

Electron-donating groups such as amino or alkoxy substituents in *para* position of TPA induce an increase of the HOMO and a decrease of I_p. Electron-withdrawing groups such as nitro or halide substituents in *para* position mainly change the LUMO position.[4,5,12] Table 1 gives the representative calculated values for differently *para*-substituted triphenylamine derivatives. Pan *et al*. found a correlation between Hammett parameters, calculated ionization potentials and HOMO levels for several mono and multi-substituted molecules.[29]

Table 1

The electrochemistry of this class of molecules has been extensively studied through the years.[30–35] The one-electron oxidation of TPA generates a radical cation which is unstable as a consequence of the high spin density at the *para* position and undergoes dimerization to *N*,*N*,*N'*,*N'*-tetraphenylbenzidine (TPB). This EC mechanism for the electrochemically induced dimerization of TPA to TPB is shown in Scheme 1. It involves a chemically irreversible coupling of two radical cations ($TPA^{\cdot+}$) to generate a doubly charged tetraphenylbenzidine moiety (TPB^{2+}). The process is followed by elimination of two protons and rearomatization to a neutral TPB. The dimer is more easily oxidized than the corresponding monomer. In the potential range of TPA radical cation formation, TPA is therefore instantaneously oxidized to the dication over its radical cation.

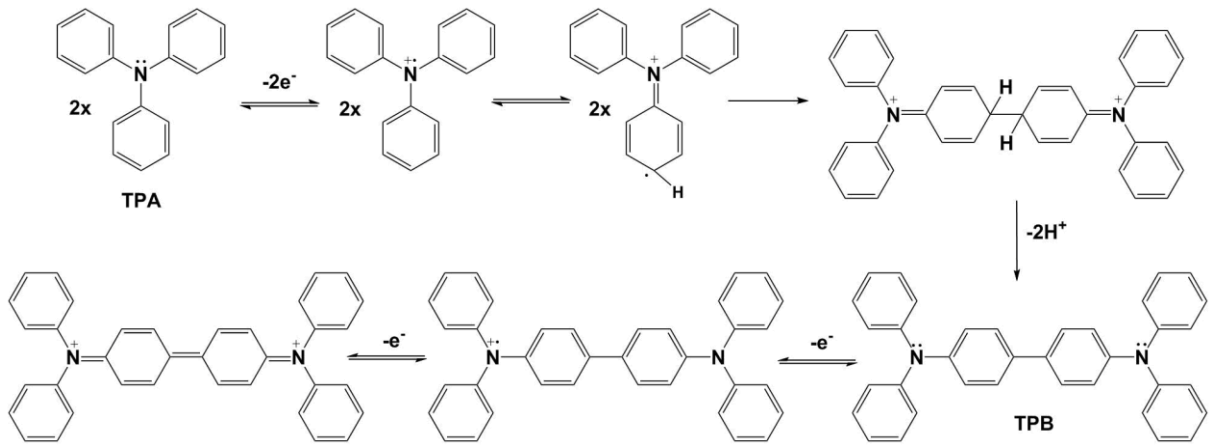

Scheme 1: Mechanism towards TPB formation upon electrochemical oxidation of TPA.

Figure 2 shows the two first voltammetric cycles measured of a TPA solution[34]; the different peak patterns obtained for the two cycles are evidence of the dimerization of TPA to TPB. In the first oxidation scan only one high peak at 0.69 V *vs* Fc/Fc^+ is observable. This peak can be associated to the chemically irreversible oxidation of TPA to its radical cation, which undergoes in the time scale of the experiment a follow up reaction to TPB. In the same potential range for which the radical cation of TPA is formed, the more conjugated dimer is immediately oxidized to its dicationic state. In the reverse voltammetric sweep the so formed TPB dication is reduced through two reversible steps, first to the radical cation (0.41 V) and then, for less positive potential values, to the neutral dimer (0.16 V). The reversible redox switching of the dimer is fully observable in the second voltammetric cycle. Evidence of the dimerization process is supported by spectroelectrochemical measurements (Figure 2).[34] At the beginning of the first oxidation scan, the formation of TPA radical cation, $TPA^{\cdot+}$, is associated with the appearance of absorption bands with maxima at 340 nm, 562 nm and 658 nm (see spectra at 0.52 V, Figure 2b). The increase of the oxidation potential at more positive values, which results

in a distinctive oxidation peak at 0.69 V, is associated with the formation of new bands with maxima of absorption at 484 nm and 722 nm, respectively. These bands are associated to the oxidized forms of the dimer, i.e. the radical cation $TPB^{\cdot+}$ and the dication TPB^{2+} (see spectra at 0.61 – 0.69 V, Figure 2b). A further increase of the oxidation potential leads to the disappearance of $TPA^{\cdot+}$ and $TPB^{\cdot+}$ bands with simultaneous increase of TPB^{2+} absorption (see spectra at 0.79 – 1.09 V, Figure 2b). The development of the absorption spectra in the backward scan, as the polarization potential is decreased to the initial value, shows the vanishing of TPB^{2+} absorption in favor of $TPB^{\cdot+}$and neutral dimer TPB. The absence of absorption for TPA indicates the complete reaction of its radical cations upon oxidation (Figure 2c). Electrochemical and absorption data for TPA and TPB and associated redox species upon electrochemical oxidation in solution are resumed in Table 2.

The HOMO level of TPA and TPB extrapolated from $E_{ox,I}^{p}$ (TPA) and $E_{ox,I}^{1/2}$ (TPB) values of CV measurements are -5.79 and -5.35 eV (taking 5.1 eV for Fc/Fc^{+} to relate the electrochemical scale to the energy scale), respectively, well correlating with literature values.[36]

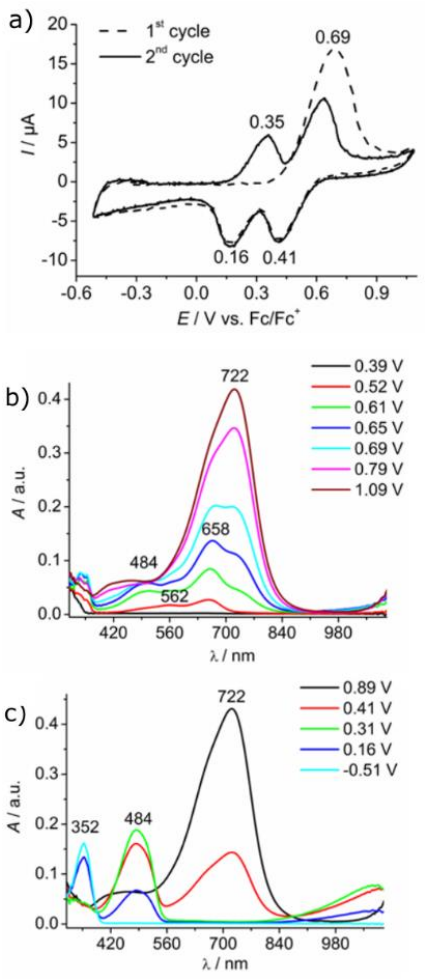

Figure 2: TPA oxidation in thin layer cell (0.1M $TBAPF_6/CH_2Cl_2$; scan rate 20 mV/s), in situ spectroelectrochemical measurements. **a)** CV measurement with *in situ* UV-vis absorption spectra recorded for the first voltammetric cycle during **b)** charging and **c)** discharging. Figures adapted from ref. 34.

Table 2

As previously stressed, TPA dimerization takes place through an oxidative coupling mechanism, a similar mechanism is found in the initial steps of electrochemical polymerization of conjugated monomers, leading to similar considerations relating to the process.[37] By analogy with π-conjugated monomers,[37–39] the electronic and steric effects of substituents in TPA *para* positions can dramatically influence the reactivity of radical

cation towards the coupling reaction.[30,40] Radical cations can be stabilized by increasing the conjugation length of the system or introducing electron donor groups such as alkyl, alkoxy or amino groups in appropriate positions.[39] Furthermore, the presence of sterically hindered substituents and the blocking of reactive sites (end-capping) is a successful strategy for preventing the coupling process.[41,42]

In this context, we compared the coupling behaviour of a set of TPA molecules, namely unsubstituted TPA and tri-*p*-tolylamine (*p*-TTA).[34] Contrary to TPA, the one-electron oxidation of *p*-TTA leads to the formation of stable radical cation species. This was evidenced by constant intensity EPR spectra for the *in-situ* generated radical cation species,[30] by a reversible oxidation pattern in CV measurements and by the presence of characteristic radical cation bands observed during *in-situ* spectroelectrochemical measurements. We could show how the oxidation of the tri-substituted TPA at the dication level leads to different chemical follow-up reactions, through two competing reaction pathways (Figure 3). The first pathway involves an irreversible intramolecular coupling reaction leading to the formation of a carbazole unit; as also reported by Nelson and coworkers.[43] The second pathway is constituted by a reversible intermolecular coupling leading to different sets of σ dimers, depending on the coupling position. These species were observed to be stable in the charged state and discharge only at relatively negative potentials. The relative amount of these follow-up products is temperature dependent. In particular, the intermolecular coupling appears to be favoured at lower temperatures due to the higher value of the dielectric constant and entropic effects.[34]

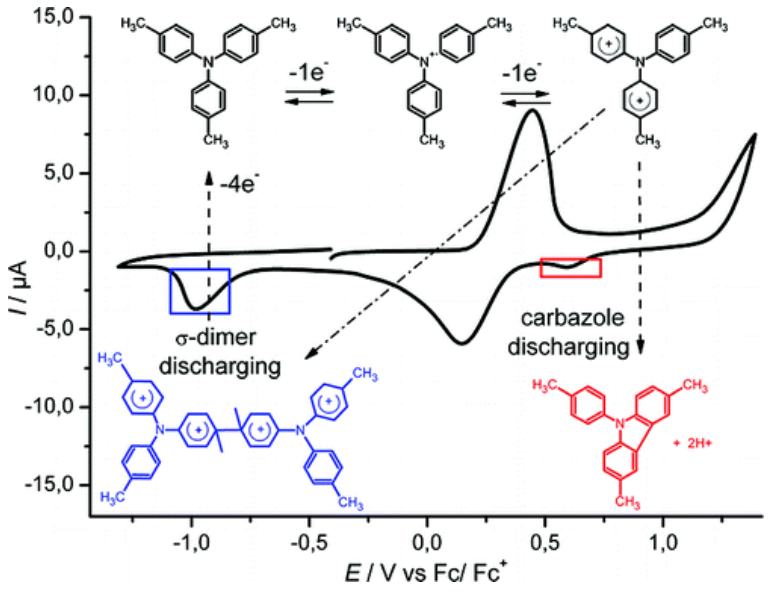

Figure 3: CV in thin layer cell of tri-*p*-tolylamine in $TBAPF_6/CH_2Cl_2$ 0.1 M, scan rate 20 mV/s, with peak assignment for the products of the reversible and irreversible follow up reactions from ref. 34.

Crosslinking in polymer films for stable redox-active films

The dimerization ability of TPA units at the level of radical cations has been also observed in polymer systems bearing electroactive TPA units as side groups.[34,44–46] In this case TPA acts as an electrochemical crosslinker upon oxidation, generating polymers modified with redox-active tetraphenylbenzidine units. In the literature one can find several examples of electrochemical crosslinking of polymers bearing covalently bound redox active pendants capable of oxidative coupling.[47,48] This approach constitutes an attractive pathway for the preparation of conductive films, as alternative to the more commonly employed deposition of chemically synthesised polymers and the electrochemical polymerizations of π-conjugated monomers. The said strategy includes in a first step the deposition of chemically synthesised polymers through solution casting methods and, in

a second step, the oxidative crosslinking/dimerization of the redox active units initiated either chemically or electrochemically resulting in crosslinked films.

We herein discuss two examples of our group on the application of TPA as redox-active crosslinking units as pendants of a polystyrene and a polythiophene backbone. Particular focus is put on the elucidation of the conductivity behavior of these redox and conjugated redox polymers respectively.

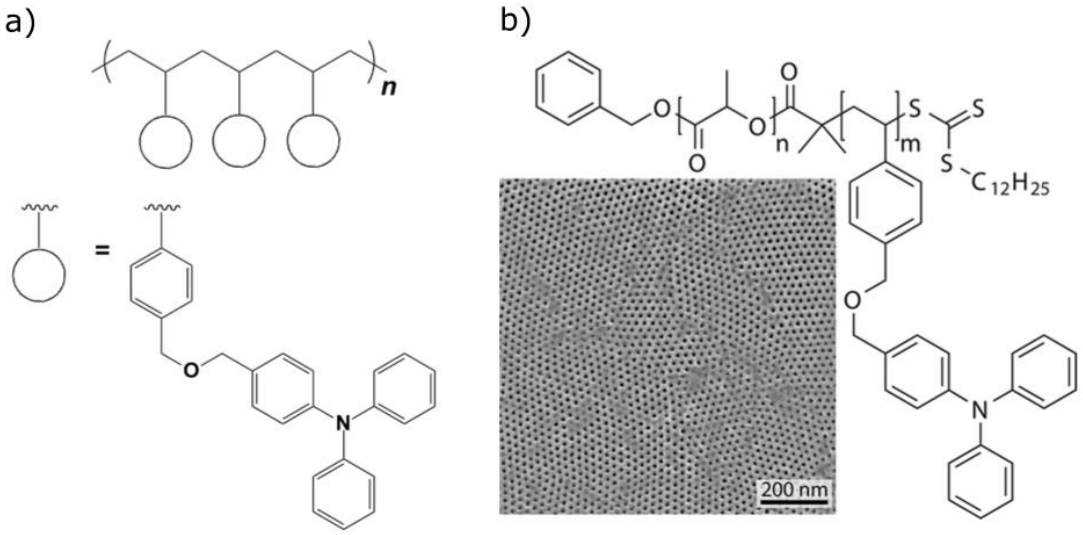

Figure 4: Chemical structures of **a)** PSTPA (ref. 44) and **b)** Chemical structure of PSTPA-*b*-PLA diblock copolymer, consisting of a triphenylamine side group polymer block and a poly(D,L-lactide) block (PLA); SEM image of the surface of an electroactive PSTPA porous template structure after PLA removal. Figure adapted from ref.36.

The polymer PSTPA (Figure 4a) is composed of a polystyrene backbone bearing TPA electroactive units attached *via* dimethyl ether spacers.[44] Thin films of this redox polymer were deposited on electrodes (ITO or interdigitated electrodes) and the coupling and conductivity mechanism upon electrochemical oxidation was investigated by means of *in situ* spectroelectrochemistry and CV coupled with conductance measurements. The CV pattern of these films is identical to TPA molecular systems, which means dimerization

into TPB systems in the first cycle and reversible redox chemistry of TPB in the second and following cycles, Figure 5a. The CV suggests full crosslinking, no free pending TPA moieties seem to remain in these films. The conductance profile in the second cycle (Figure 5b) is endowed with two independent, partially superimposing conductivity regimes associated to two discrete mixed valence states for radical cation and dication, respectively.[37,44] The conductivity behavior observed for this system at both radical cation and dication level can be described in analogy to the conductivity mechanism in radical ion salts[49] and redox polymers.[50] These systems are nonconductive both in the neutral and fully oxidized state and the charge transport is ascribed to the one electron interchain hopping process between oxidized and reduced sites of a redox state, with maximum conductivity reached for an equal number of oxidized and reduced sites. The sketch in Figure 5b highlights the conductivity regimes of inter and intra molecularly linked TPB units. In analogy to this behavior, Heinze *et al*. observed a conductivity pattern for a 3D hybrid network with sexithiophene oligomers bridging dendrimeric cores, with maximum conductivity reached for half charge level.[51]

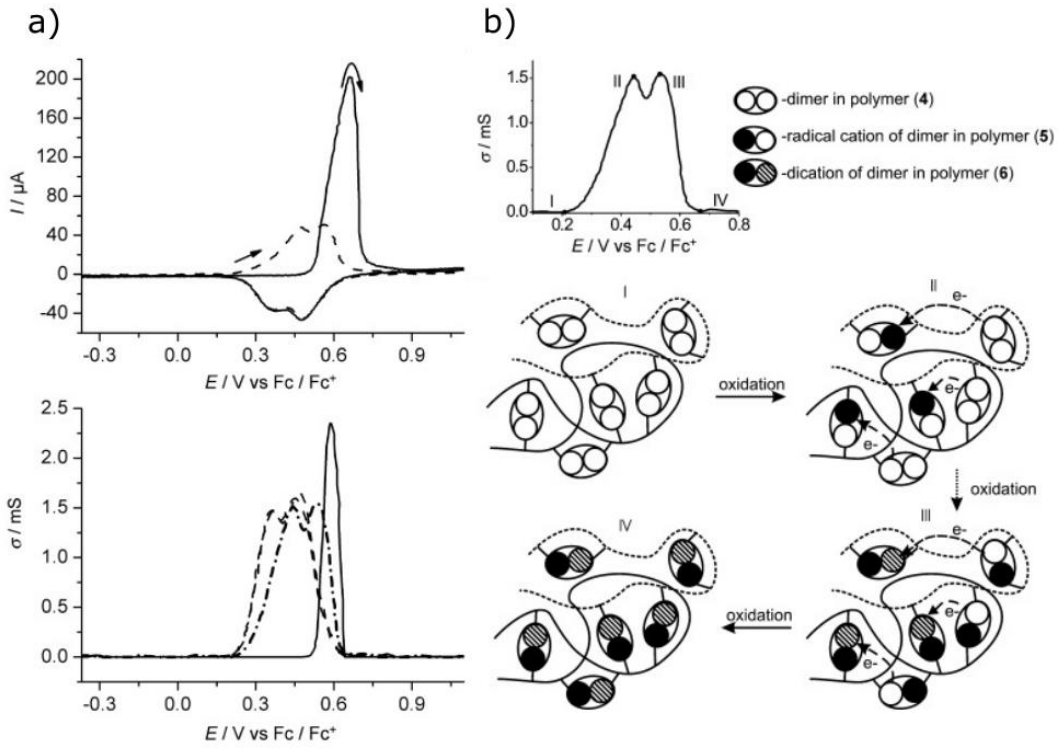

Figure 5: a) CV and *in situ* conductance measurements for PSTPA polymer films (MeCN/$TBAPF_6$ 0.1 M; scan rate 20 mV/s), first and second cycle and corresponding *in situ* conductance pattern measured simultaneously. **b)** Explanation of the respective redox species and conductivity profile in crosslinked PSTPA polymer films. Figures adapted from ref. 44.

The redox polymer PSTPA was further integrated as block into a block copolymer giving an interesting example of a microphase-separated architecture proving the versatility of this class of material.[36] With reference to earlier studies where a polystyrene-*block*-polylactide block copolymer allowed preparation of nanoporous templates for applications in perovskite solar cells,[52,53] PSTPA was connected to poly(lactide) (PLA). These PSTPA-*block*-PLA block copolymers have a cylindrical bulk morphology, with PSTPA constituting the majority component. Polymer films characterized by perpendicularly oriented cylinders at the surface and a tortuous inner structure are spontaneously formed directly after spin casting (Figure 4b). The cylinders have a center-

to-center distance of 21 ± 2 nm and an average diameter of 13 ± 2 nm. The employment of PLA block allows its degradation through mild hydrolysis conditions,[54,55] leading to a nanoporous structure in the PSTPA semiconducting matrix. After etching, the obtained porosities can be further functionalized through the filling of the whole pore structure with diverse types of materials, also exploiting TPA electroactivity and crosslinking into TPB.[56]

The second polymer, namely PT-TPA, constitutes of a linear regioregular polythiophene backbone bearing TPA redox pendants connected to the main backbone *via* click chemistry[57] (Figure 6). Films can be prepared by classical solution deposition, *e.g*. spin-coating. The dimerization ability of the pendant TPA was exploited for post deposition crosslinking and its effects on film absorption, redox and conductivity characteristics were analyzed. In PT-TPA thin films, the oxidation potential of TPA/TPB redox units and of the polythiophene backbone falls in the same region, resulting in the simultaneous generation of charge carriers. One can talk about redox-matching in this context. CV measurements and *in situ* spectroelectrochemistry on solution-cast PT-TPA films give evidence of the successful dimerization of TPA to TPB into crosslinked films. Figure 6a shows the CV of such a crosslinked PT-TPA film. The corresponding conductance profile reveals a plateau-like pattern which is similar to the one found in literature for many conjugated polymers[37] and confirms the supremacy of the thiophene conjugated backbone in determining the conductivity characteristics, (see Figure 6a). However, *in situ* spectroscopy also clearly shows the oxidized species of TPB which means they do contribute to the overall conductivity. Based on these findings a classification into conjugated redox polymers is well suitable.

Motivated by successful electrochemical doping, we also explored chemical doping strategies. We could show how post deposition modification of PT-TPA films involving

TPA oxidative coupling (*i.e*. crosslinking) can be successfully performed through the employment of chemical oxidants. In literature the polymerization and doping of polythiophenes as well as triphenylamine and carbazole polymerization could be induced by $FeCl_3$.[58,59] When using $FeCl_3$ as oxidizing agent for PT-TPA, the effectiveness of crosslinking was evidenced by the appearance of bands associated to TPB and its doped forms $TPB^{\cdot+}$ (λ_{max} ~ 465 nm) and TPB^{2+} (λ_{max} ~ 757 nm) together with the ones of polythiophene backbone charging with $PT^{\cdot+}$ (λ_{max} ~ 837 nm) and PT^{2+} (λ_{max} ~ 1050 nm) species. This is in analogy to what was detected during *in situ* spectroelectrochemical measurements. The use of such an oxidizing agent leads therefore to the simultaneous crosslinking and doping of the polymer film, similarly to the electrochemical process. The variations brought by chemically induced oxidative crosslinking and doping on PT-TPA conductivity were also analyzed by means of four-point probe measurements, revealing high conductivity values of 8 ± 2.1 $S \cdot cm^{-1}$ for PT-TPA doped *via* $FeCl_3$ (Figure 6b).

Crosslinking was also associated to a significant decrease of solubility, making the polymer films insoluble in different organic solvents, from which non-crosslinked films could be solubilized. Post-deposition crosslinking becomes therefore an interesting approach for applications employing organic solvents, and for which dissolution of the active material is a limiting factor. We envision that the simultaneous crosslinking and doping might be a new concept for the preparation of hole-transport layers in OPV or OLEDs as well as organic thermoelectric devices.

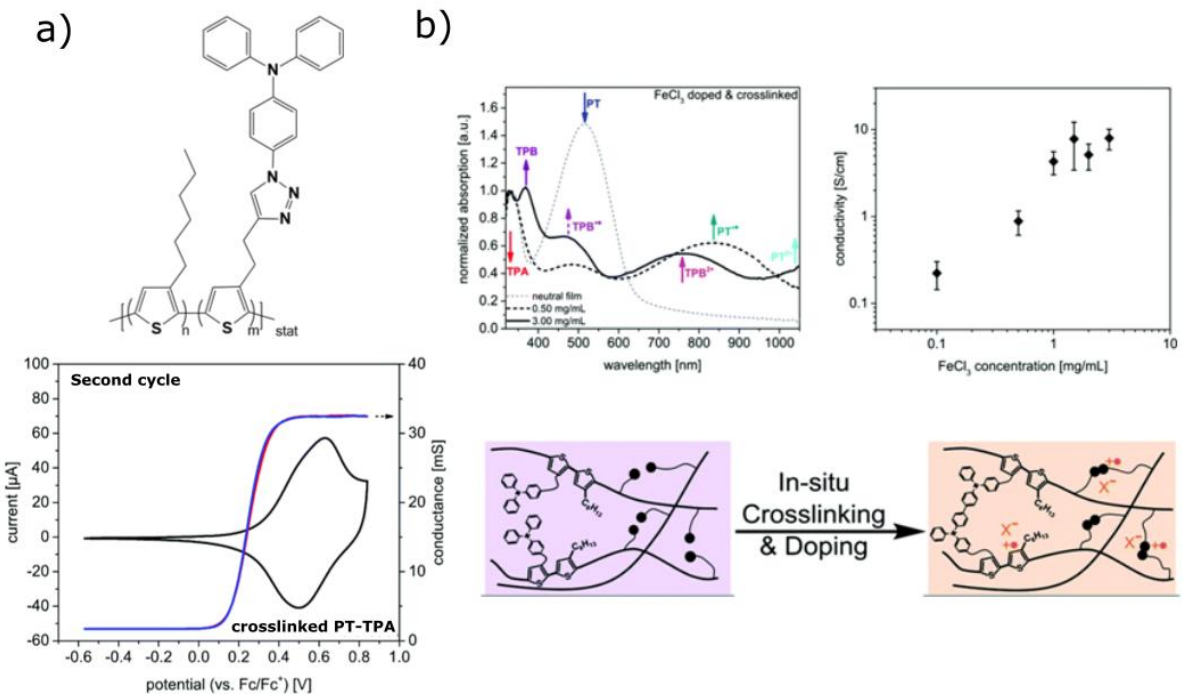

Figure 6: a) CV and *in* situ conductance measurement for a crosslinked PT-TPA thin film **b)** Absorption spectra and conductivity measurements of crosslinked PT-TPA for different dopant solution ($FeCl_3$/$CHCl_3$) concentrations. Figures adapted from ref. 57.

Triphenylamine-based push-pull molecular donors for organic photovoltaics

D-π-A push-pull molecules based on TPA or aryl derivatives as electron-donating blocks (D) connected *via* a π-spacer to various electron-withdrawing blocks (A), have been widely developed as electron-donor materials for OPV. Their combination with electron-acceptor materials such as fullerene derivatives *via* solution or vacuum processing allows the elaboration of efficient planar heterojunction (PHJ) or bulk-heterojunction (BHJ) organic solar cells (OSCs).[10–12] These push-pull donors can be divided in three main classes depending on their structure, namely star-shaped DA_3, DAD and linear DA molecules.

Star-Shaped DA_3 push-pull molecules

The development of star-shaped TPA-based push-pull molecules as donor materials in OSCs was pioneered by Roncali and co-workers.[60–63] One of the first examples, namely **DA_3-1**, was reported in 2006 (Figure 7).[60,61] This DA_3 compound exhibits a central TPA functionalized with three thienyl (T)-dicyanovinyl (DCV) branches at each *para* position of the benzene rings. The propeller shape of TPA imparts a 3D character to **DA_3-1** which is expected to produce amorphous materials with isotropic electronic properties. Bilayer OSCs associating **DA_3-1** with C_{60} as electron-acceptor (ITO/PEDOT-PSS/**DA_3-1**/C_{60}/LiF/Al), led to a power conversion efficiency (*PCE*) of 1.85 % (at 80 mW under AM 1.5 simulated solar irradiation). Few years later, the introduction of a hybrid anode buffer layer MoO_3/CuI led to a *PCE* of 2.50 %.[64]

The introduction of the electron-withdrawing DCV units in **DA_3-1** creates an efficient intramolecular charge transfer (ICT) between the electron-donating D and electron-accepting A units leading to a broad absorption band in the visible spectrum (λ_{max} = 509 nm) (Figure 7). In addition, the DCV units induce an increase of the oxidation peak potential of **DA_3-1** (E_{pa}^1 = 0.64 V *vs* Fc/Fc^+) corresponding to a deeper HOMO level which in turn i) produces an exceptionally high open-circuit voltage (V_{oc} = 1.15 V) for the bilayer OSC, and ii) provides also a better stability of molecule **DA_3-1** towards oxygen. The cyclic voltammogram (CV) of **DA_3-1** shows a reversible oxidation wave in agreement with a stable radical-cation species. Compared to the high reactivity of the radical cation of TPA, as described above, the insertion of terminal groups at the *para* position of each phenyl ring combined with the π-extension of the arms favour the stabilization of the radical cation

species hence preventing any follow-up dimerization of electropolymerization reactions. Note that compound **DA$_3$-1** displays also an irreversible reduction peak at E_{pr}^1 = -1.65 V.

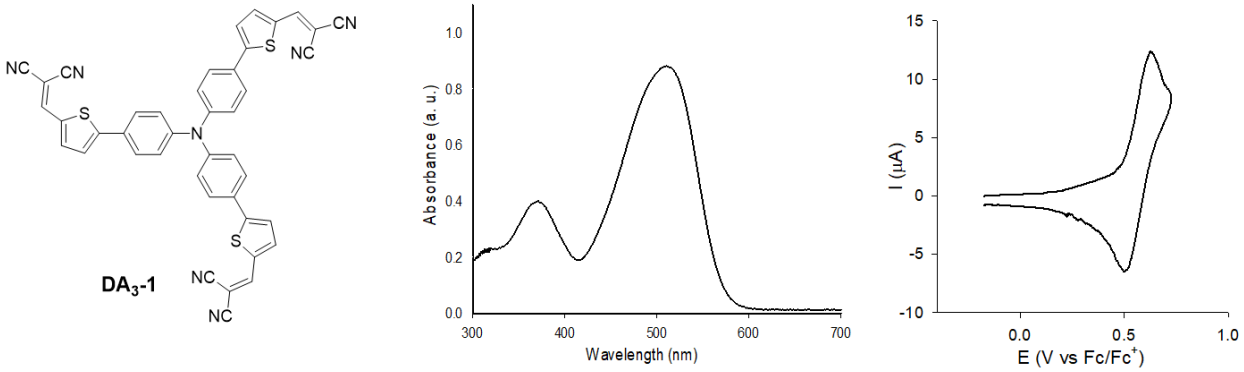

Figure 7: Structure of **DA$_3$-1** (left), UV-vis spectrum in CH_2Cl_2 (middle) and CV in 0.1 M Bu_4NPF_6/CH_2Cl_2 (right), Pt counter and working electrodes, scan rate 100 mV/s. Adapted from ref 60.

Since then, many other DA_3 push-pull molecules derived from TPA have been successfully used as donor materials in BHJ OSCs in the presence of $PC_{71}BM$ as acceptor material.[11,12] Scheme 2 shows representative examples. Brabec, Ponomarenko and co-workers synthesized a series of star-shaped molecules similar to **DA$_3$-1** with alkyl-substituted DCV end groups and different oligothiophene π-spacers.[65,66] For instance, BHJ OSCs fabricated from **DA$_3$-2** gave a high *PCE* of 4.72 % due to the favourable film morphology of the blend with $PC_{71}BM$ and to the exceptionally high hole mobility (μ_h = 3.99 × 10^{-3} cm^2 V^{-1} s^{-1}) measured on thin-films of **DA$_3$-2** by the space charge limited current (SCLC) method.[65] Li *et al*. introduced an electron-deficient benzothiadiazole unit inside each oligothiophene arms leading to **DA$_3$-3** that gave a BHJ OSC with *PCE* of 4.3 %.[67] By introducing a fluorine atom on the benzothiadiazole unit to increase its electron affinity and insertion of an electron-rich dithienosilole block to extend the conjugation length of each arm, Ko *et.al.* reported the synthesis of **DA$_3$-4** and further improved the

PCE up to 4.7 %.[68] More recently the diketopyrrolopyrrole (dpp)-based star-shaped molecule **DA$_3$-5** was described showing that the nature of the alkyl chains of the dpp has a strong impact on the supramolecular self-assembly. When a branched 2-ethylhexyl chain was used, thin-films showed crystalline domains whereas dodecyl chains in **DA$_3$-5** promoted the formation of one-dimensional nanowires beneficial for the PV performance of BHJ OSCs, *PCE* increasing respectively from 2.9 % to 4.4 %.[69]

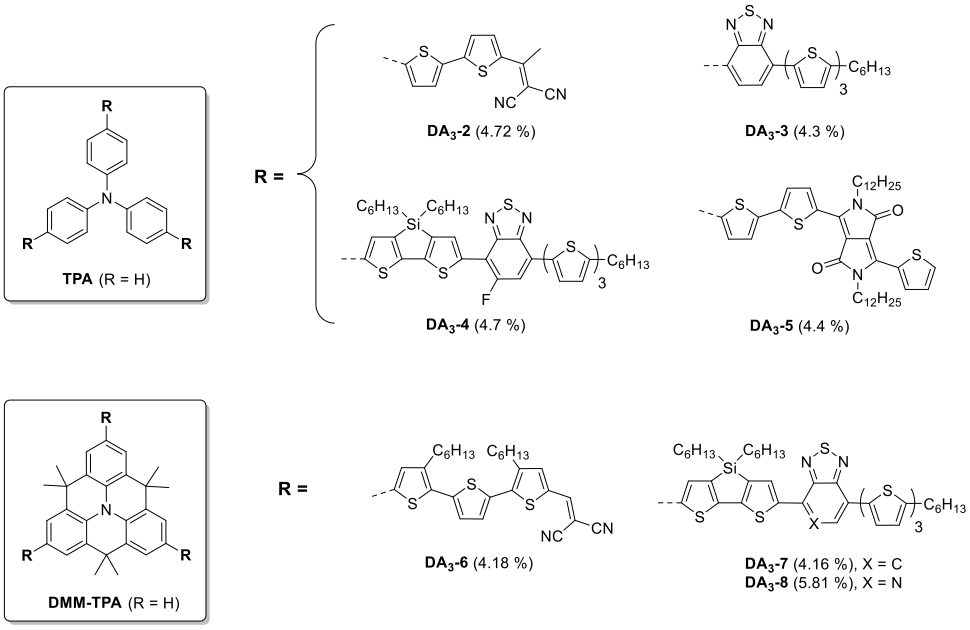

Scheme 2: Representative examples of TPA-based DA_3 push-pull donors and *PCE* values of $PC_{71}BM$-based BHJ single junction OSCs.

Star-shaped push-pull molecules with a central dimethylmethylene TPA-bridged core (DMM-TPA) as active material for OPV have been described by the group of Ko.[68,70–72] X-ray diffraction data on a single crystal of DMM-TPA show that the dihedral angles between phenyl rings and the plane of the three N-bonded carbon atoms are much smaller in DMM-TPA (ca. 5.9° and 7.6°) than those of TPA (> 43°).[73] As determined by square wave voltammetry,[74] the oxidation potential of DMM-TPA is negatively shifted by *ca* 0.2 V

compared to that of TPA due to its planarized structure combined with the presence of alkyl substituents in *ortho* positions of the benzene ring. In addition, the reversibility of the oxidation wave of DMM-TPA shows an enhanced stability for the radical cation,[74] even making possible the access to radical cation salts.[75] Thus, DMM-TPA is expected to improve intramolecular π-electronic delocalization and favour intermolecular interactions resulting in increasing hole mobility and PV performance. BHJ OSCs with **DA_3-6** with three arms based on terthiophene bridge end-capped with a DCV unit, gave a *PCE* of 4.18 %.[71] Compound **DA_3-7** with arms including a dithienosilole and a benzothiadiazole unit shows in solution an ICT band at 543 nm which is red-shifted by 2 nm compared to its TPA analogue whereas this shift increases to 20 nm for thin-films.[70] The HOMO level of **DA_3-7** (- 5.24 eV) slightly increases as compared to that of the TPA counterpart (- 5.29 eV). The best BHJ OSCs with **DA_3-7** gave a *PCE* of 4.16 %, higher than the value obtained in the same conditions for the TPA analogue (*PCE* = 3.49 %). This improvement was attributed to the efficient intermolecular π-π packing interactions and to the enhanced hole mobility of **DA_3-7**. Remarkably, the replacement of the benzothiadiazole unit by a thiadiazolopyridine ring in **DA_3-8** has led to BHJ OSCs with a maximum *PCE* of 5.18 % which is again higher than the one obtained for the TPA analogue (*PCE* = 3.88 %) and represents one of the highest *PCE* ever reported for a DA_3 system.[72]

DAD push-pull molecules

TPA-derived push-pull molecules with a DAD structure have also been investigated for OPV. Their synthesis relies on mono-functionalized TPA which makes the synthesis easier. The choice of the electron-deficient core A can significantly affect the PV performance although the architecture of the devices plays also a crucial role. Several solution-processable (X = 1-5) and vacuum-deposited (X = 6,7) **DAD-X** systems leading to OSCs with high *PCEs* are represented in scheme 3. The dicyanomethylenepyrane (**DAD-1**),[76] thieno[3,4-c]pyrrole-4,6-dione (**DAD-2**)[77] or thiazolothiazole (**DAD-3**)[78] derivatives were combined with $PC_{71}BM$ to prepare BHJ with *PCE* of 2.10 %, 3.31 % and 4.05 % respectively. This improvement is due to the nature of the electron-deficient unit A and also to the progressive π-extension of the conjugated bridge between the TPA and A. As developed by Li *et al*., one approach consists in using a central electron-deficient benzothiadiazole flanked with different π-extended systems.[79] Thus a *PCE* of 4.86% was obtained with a BHJ combining $PC_{61}BM$ and **DAD-4** that exhibits a fluoro-substituted benzothiadiazole ring.[80]

The groups of Wong and Forrest have been particularly interested in vacuum-processed planar heterojunction OSCs. For example, the small **DAD-6** molecule with one rigid fluorenylidene malononitrile core was used for preparing co-evaporated BHJ with C_{60} or C_{70}, giving a *PCE* of 3.12 % and 4.04 %.[81] On the other hand, Forrest *et al.* have developed squaraine derivatives such as compound **DAD-7** for bilayer OSCs with C_{60} which upon thermal annealing produce 5.2 % efficiency.[82,83] It is worth noting that a further increase of *PCE* up to 5.7 % has been achieved by replacing the TPA units by a *N*,*N*-

diphenylnaphthalen-1-amine that favours π-stacking and hence, improved charge transport and exciton diffusion.

Finally, solution-processed BHJ OSCs based on **DAD-5** gave a high *PCE* reaching 6.13%; this benzothiadiazole derivative is indeed a $D_1AD_2AD_1$ system with a central electron-rich dithienobenzene flanked by two alkylated thiophene substituents.[84]

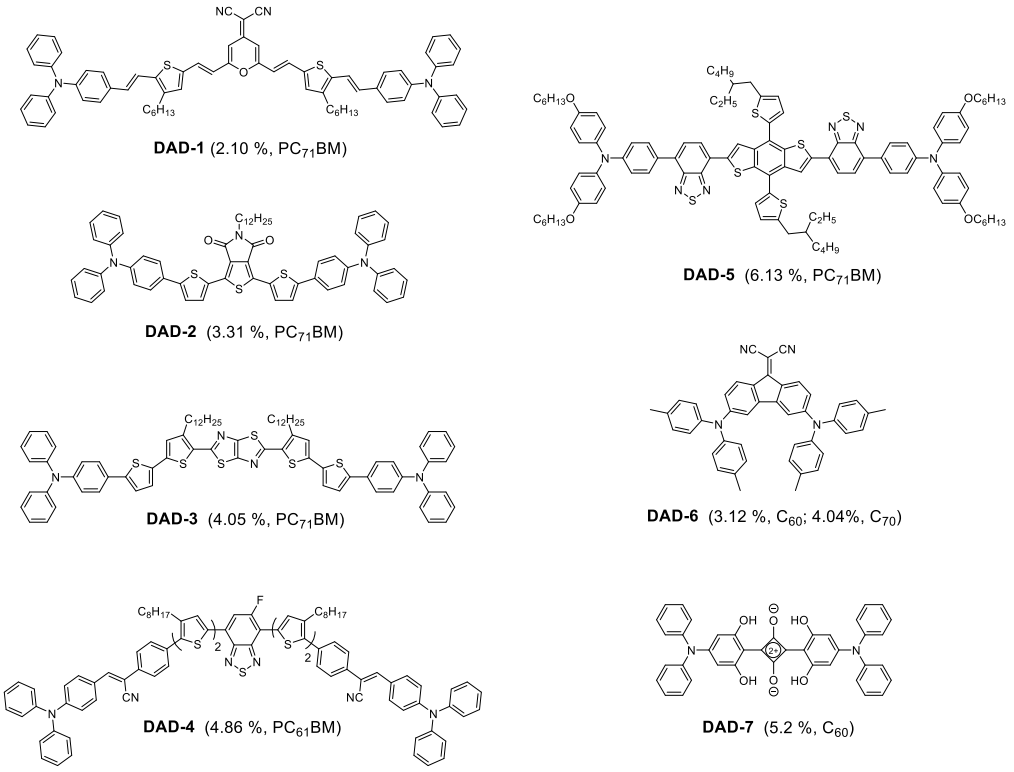

Scheme 3: Representative examples of TPA-based DAD push-pull donors and related *PCE* of single junction OSCs.

Our group has developed a series of DAD systems (**DAD-8**) based on 1,1,4,4-tetracyanobuta-1,3-diene (TCBD) as a new electron-accepting group A for OPV (Figure 8).[85] The latter was used in 2001 by Jen *et al*. in dipolar D-π-A chromophores for application in nonlinear optics.[86] The chemistry of TCBD was further explored by the group of F. Diederich.[87] The TCBD moiety is easily obtained *via* a [2+2] cycloaddition between tetracyanoethylene and acetylene derivatives preferably substituted by electron-releasing

substituents, this “click”-type reaction is highly efficient and, in principle, does not produce by-products.

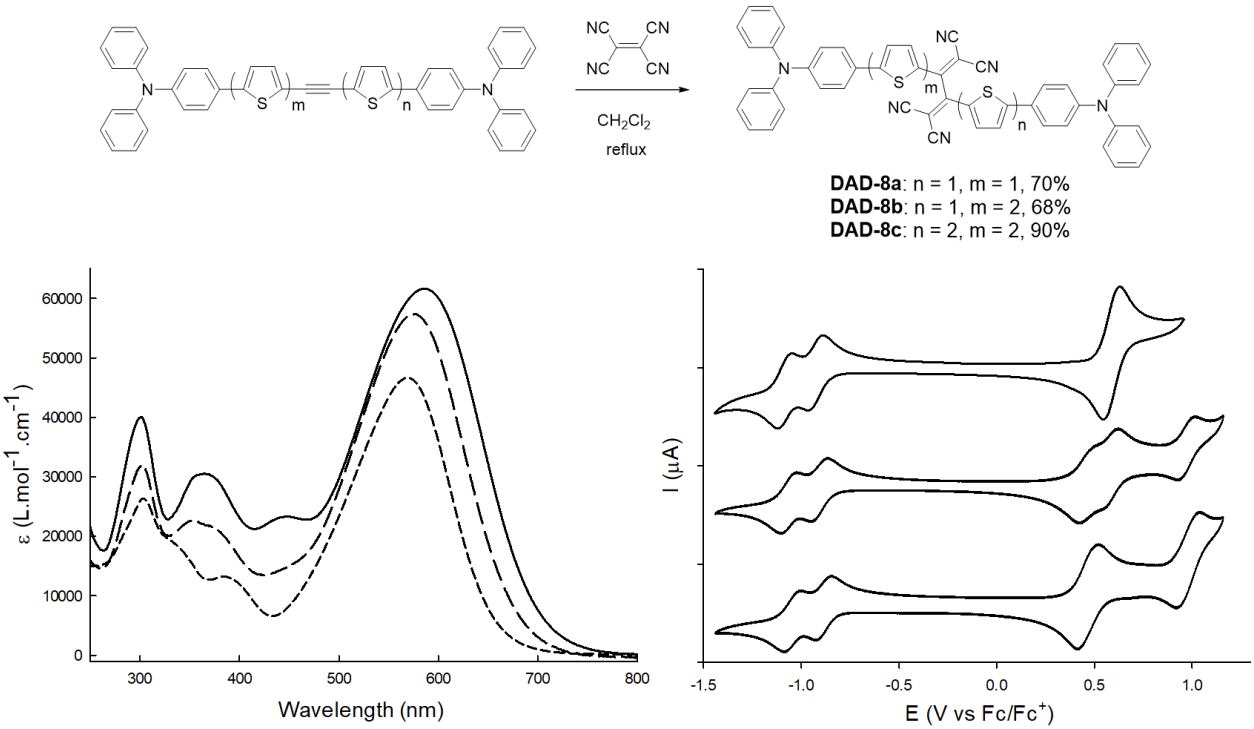

Figure 8: Synthesis of **DAD-8**. Left: Absorption spectra of **DAD-8a** (solid line), **DAD-8b** (long dashed line) and **DAD-8c** (short dashed line) in CH_2Cl_2. Right: CVs of **DAD-8a** (top), **DAD-8b** (middle) and **DAD-8c** (bottom) 0.5 mM in 0.1 M Bu_4NPF_6/CH_2Cl_2, Pt working electrode, scan rate 100 mV/s. Adapted from ref. 85.

The UV-vis spectra of compounds **DAD-8** show an intense broad ICT band that shifts from 569 nm for **DAD-8a** to 576 nm and 586 nm for **DAD-8b** and **DAD-8c**, respectively, in agreement with the progressive extension of the π-conjugation (Figure 8, left).

The CV of **DAD-8a** (Figure 8, right) exhibits a two electron reversible oxidation wave with anodic peak potential E_{pa}^1 at 0.63 V *vs* Fc/Fc^+ assigned to the simultaneous one-electron oxidation of the two lateral thienyl-TPA branches. The CV of **DAD-8a** shows also two successive one-electron reduction waves at E_{pr}^1 = - 0.97 V and E_{pr}^2 = - 1.13 V associated to the reduction of the central strong electron-withdrawing TCBD unit; close

values are observed for **DAD-8b** and **DAD-8c**. On the other hand, the lengthening of the oligothiophene chain in **DAD-8b** and **DAD-8c** induces a negative shift of E_{pa}^{1} with the appearance of additional oxidation peaks at more positive potentials. In particular, the CV of the unsymmetrical compound **DAD-8b** shows three one-electron reversible oxidation waves peaking at 0.51 V, 0.62 V and 1.02 V. The first and the second processes are assigned to the successive oxidation of the bithienyl- and thienyl-TPA branches to the radical cation whereas the third one can be related to the oxidation of the bithienyl-TPA branch to the dication state. These electrochemical results, in agreement with the small red shift of 17 nm from **DAD-8a** to **DAD-8c**, suggest a relatively weak intramolecular electronic interaction between the two lateral conjugated arms through the central TCBD segment. These experimental results agree well with the DFT-optimized geometry of molecules **DAD-8** which exhibit significant dihedral angles of 93-96° between the planes containing the two DCV groups of TCBD (Figure 9).

Bilayer OSCs were fabricated from a solution-processed thin-film of **DAD-8a** leading to a *PCE* of 1.08 %, a short-circuit current density J_{sc} of 3.06 mA cm^{-2}, an open-circuit voltage V_{oc} of 0.97 V and a fill-factor *FF* of 0.33 for the best device. This high V_{oc} value can be related to the relatively low HOMO energy level of **DAD-8a**. Enhanced performance (*PCE* = 1.72 %) was obtained with the extended derivative **DAD-8c** in the same conditions while the use of C_{70} led to *PCE* higher than 2 % for both compounds **DAD-8a** and **DAD-8c**.

With the idea of increasing the scalability and limiting the economic cost and the environmental impact of the synthesis of organic materials for potential industrial application in OPV,[88] Leriche and co-workers from our group have developed the straightforward synthesis of **DAD-9** based on a central diiminofumaronitrile acceptor

group (Scheme 4). This compound was prepared in few steps in good yield by double condensation of a TPA-carbaldehyde derivative with 2,3-diaminomaleonitrile under microwave activation with trifluoroacetic acid (TFA) as catalyst.[89] The photovoltaic potential of **DAD-9** was evaluated in bilayer OSCs with C_{60} leading to a 1.18 % efficiency. Following a similar approach, Frère and co-workers described the Schiff base **DAD-10** with a central electron-deficient benzodifurane core and corresponding bilayer OSCs with C_{60} reaching a maximum *PCE* of 1.73 %.[90]

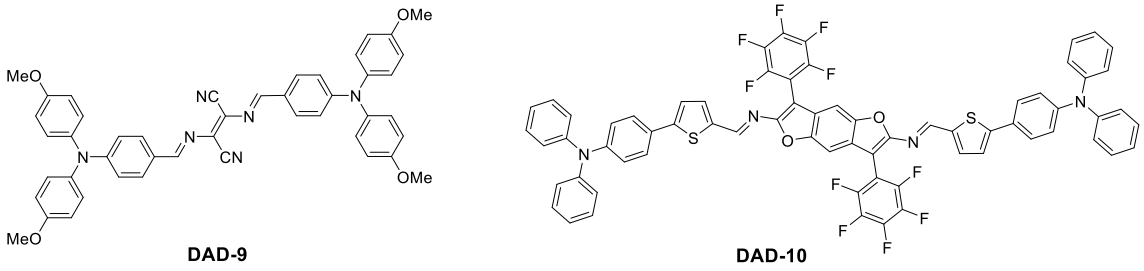

Scheme 4: TPA-based DAD push-pull donors derived from Schiff bases.

Linear DA push-pull molecules

Compared to previous systems with higher dimensionality, smaller linear DA push-pull molecules have an increased tendency to form aggregates and crystallize which can improve the charge transport properties of related thin-films. They generally present the advantage to be processed in solution or by vacuum deposition leading to homogenous thin-films for the elaboration of bilayer heterojunction or BHJ OSCs.

Scheme 5 shows selected examples of TPA-based DA push-pull molecules for OPV. Compound **DA-1** represents one of the first examples reported for OPV.[91] The π-spacer between A and D was extended by connecting the nitrogen of TPA to a fluorenyl unit functionalized by a quaterthiophene backbone end-capped with an electron-

withdrawing DCV unit. A *PCE* of 2.67 % was obtained for a bilayer OSC with C_{60}. Ko *et al*. developed **DA-2** based on a shorter bithiophene spacer and a modified-TPA with two outermost fluorenyl units, for solution-processed BHJ with $PC_{71}BM$ affording up to 3.66% efficiency.[92] The use of a bridged dithienosilole π-spacer by the group of Wong in **DA-3** led to better electronic delocalization resulting in a red shift of the absorption band and a higher extinction coefficient.[93] BHJ prepared by co-evaporation of **DA-3** and C_{70} gave a *PCE* of 3.82 %. Extending our initial approach based on the reduced-size **DA-10** molecule (see below), Pshenichnikov *et al*. synthesized **DA-4** with an additional phenyl ring on the DCV unit. Compound **DA-4** demonstrated extremely long exciton diffusion lengths exceeding 25 nm in vacuum-deposited films and was co-evaporated with C_{70} giving BHJ OSCs yielding a *PCE* as high as 5.11 %.[94]

Again the group of Wong developed a series of push-pull molecules with the general structure DA'A by inserting an additional electron-deficient unit A', such as a pyrimidine or a benzothiadiazole. This strategy was highly successful as shown by the PV performance reported for co-evaporated BHJ OSCs with C_{70} prepared with **DA-5** (*PCE* = 6.4 %),[95] **DA-6** (*PCE* = 5.81 %)[96] or **DA-7** (*PCE* = 6.8 %).[97] More recently Wong, Kim and co-workers described efficient vacuum-deposited ternary OSCs reaching a *PCE* of 8.02 %, after optimization of the composition and the thickness of the photoactive layer prepared by co-evaporation of C_{70}, **DA-6** and **DA-8** exhibiting a thienothiophene-thiazole segment.[98] A broad absorption over the whole visible spectrum was achieved thanks to the complementary absorption of thin-films of the two donors **DA-6** (λ_{max} = 670 nm) and **DA-8** (λ_{max} = 530 nm). Note that in this work, binary OSCs with **DA-6** or **DA-8** and C_{70} gave the same *PCE* of 6.52 %.

In parallel, Forrest *et al.* thoroughly investigated the PV potential of molecules described by Wong, namely **DA-6** and **DA-7**. After preparing a single junction OSCs based on co-evaporation of **DA-6** and C_{60} (*PCE* = 5.3 %), further improvement was achieved using the photoactive layer **DA-6**:C_{60} as front subcell in a tandem cell (*PCE* = 10.0 %) and as middle subcell in a triple junction OSC (*PCE* = 11.1 %).[99] Very recently the same group has reported the highest ever reported *PCE* for an organic solar cell, namely 15.0% for an organic tandem OSC of 2 mm^2 active area, combining vacuum- and solution-processed subcells.[100] Herein a layer of co-evaporated **DA-7** and C_{70} was used for the front subcell while the back subcell consisted in a blend of donor polymer PCE-10 and ITIC, a non-fullerene acceptor based on indacenodithieno[3,2-b]thiophene, exhibiting both complementary optical properties.

Finally, Mishra, Bäuerle and Sharma and co-workers have recently described a soluble TPA-heteropentacene-DCV **DA-9** with a small bandgap of 1.59 eV and prepared BHJ with $PC_{71}BM$. The initial *PCE* of 3.34 % was improved after successive optimizations of the active layer by adding 0.3 vol % 1,8-diiodooctane (*PCE* = 6.31 %) and thermal annealing (*PCE* = 7.26 %).[101] All these results show that TPA-based linear DA push-pull molecules have progressively acquired a prominent place among other classes of donor materials for OPV.

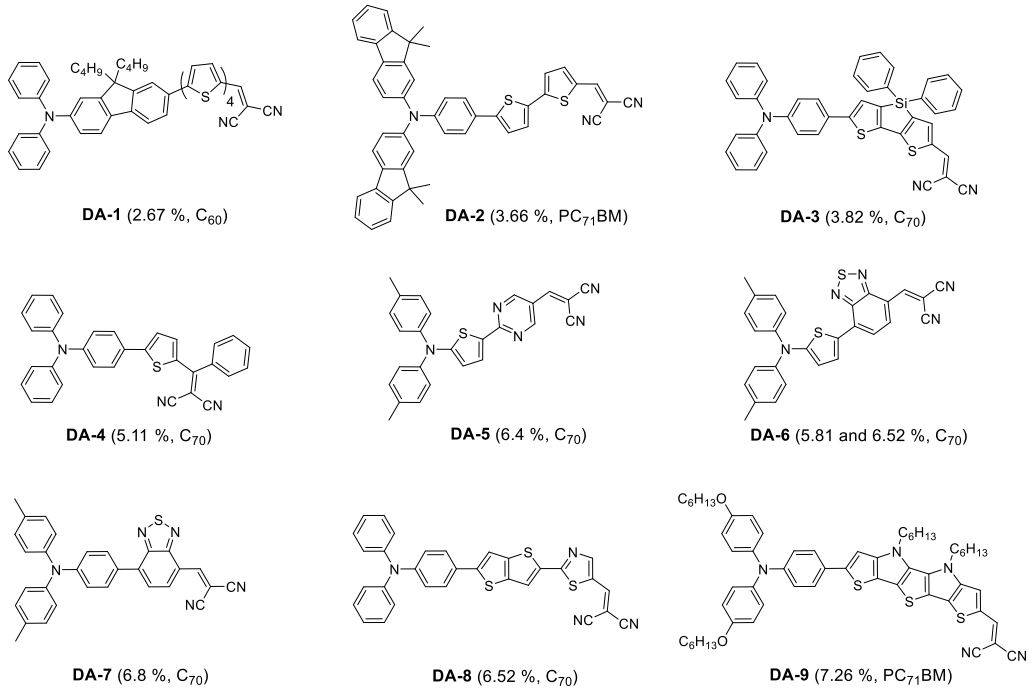

Scheme 5: Representative examples of TPA-based DA push-pull donors and *PCE* values of single-junction OSCs

Our group has developed a large number of small linear DA push-pull molecules for OPV since 2009. Owing to the significantly twisted structure of the TCBD derivative **DAD-8a**, its half structure, namely molecule **DA-10**, was first investigated for OPV (Figure 9). Initially prepared in only three chemical steps involving a Pd-catalyzed Stille cross-coupling,[102,103] the synthesis of **DA-10** was further optimized by starting from commercial 4-bromotriphenylamine and using a direct C-H arylation reaction, avoiding the use of toxic stannyl derivatives, followed by a Knœvenagel condensation.[104] Thus **DA-10** combines a simple, clean and scalable synthesis. The maximum of absorption of **DA-10** (λ_{max} = 501 nm) in solution is subjected to a 64 nm hypsochromic shift compared to that of **DAD-8a** in agreement with the weaker electron-withdrawing character of DCV compared to TCBD. Accordingly, the CV of **DA-10** exhibits a reversible one electron oxidation wave peaking at E_{pa}^{1} = 0.59 V *vs* Fc/Fc^{+}, a value which is slightly shifted towards negative potential

compared to **DAD-8a** (E_{pa}^1 = 0.63 V). This structural change induces also the irreversibility of the reduction wave of **DA-10** observed at the same value that the star-shaped molecule **DA$_3$-1** (E_{pr}^1 = - 1.65 V). Comparison of the electrochemical data of **DAD-8a** and **DA-10** shows clearly that while the HOMO levels are close, the LUMO level of **DA-10** is significantly destabilized which can account for the higher HOMO-LUMO gap observed by absorption spectroscopy. Thin-films of **DA-10** were easily prepared by solution-processing and used to fabricate a bilayer device ITO/PEDOT-PSS/ **DA-10**/C_{60}/Al with a *PCE* of 2.53 %, a higher value than the ones recorded for **DA$_3$-1** and **DAD-8a**.[61,85] This result showed that simplified and size-reduced structures could give rise to easily accessible and efficient molecular donors for OPV.

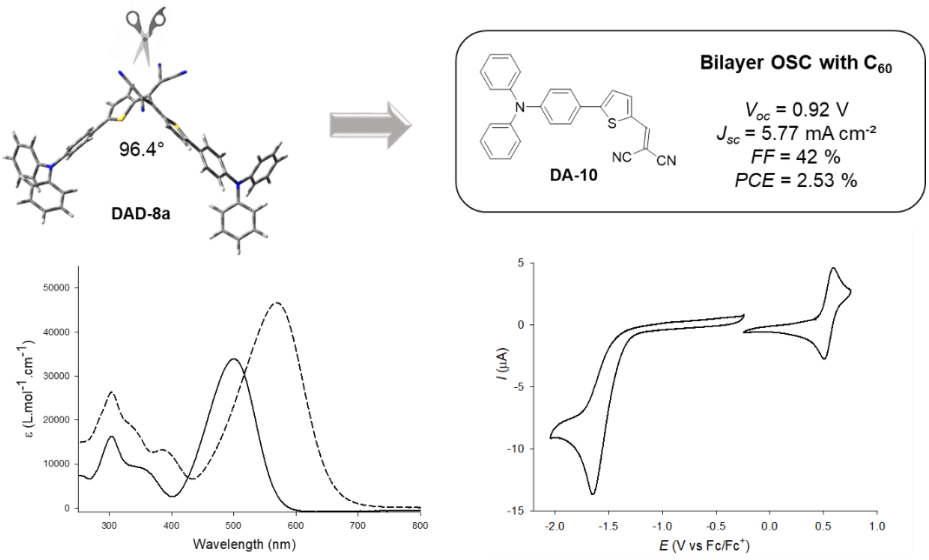

Figure 9: DFT-optimized geometry of **DAD-8a** (Gaussian 09 B3LYP/6-31G(d,p) level) and structure of **DA-10** corresponding to half of **DAD-8a** and related photovoltaic performance (Top). Absorption spectra of **DAD-8a** (dashed line) and **DA-10** (solid line) in CH_2Cl_2 (bottom left) and CV of **DA-10** 0.5 mM in 0.1 M Bu_4NPF_6/CH_2Cl_2, Pt working electrode, scan rate 100 mV/s (bottom right).

Device optimization by thermal treatment of bilayer OSCs prepared by successive *vacuum*-deposition of **DA-10**, using C_{70} instead of C_{60} for better absorbing properties in

the visible spectrum and an additional Ca interlayer and Al led to a *PCE* of 3.70 %.[103] An increased *PCE* of 4 % was obtained in a multi-layer co-evaporated BHJ OSC using **DA-10** and C_{60}, the V_{oc} reaching an exceptionally high value of nearly 1 V and the relatively high *FF* value of 64 % was associated with good charge extraction at the electrodes (Figure 10). The hole-transport properties of evaporated thin-films of **DA-10** were also analysed by the SCLC method giving a hole mobility of μ_h of 1.0×10^{-5} cm^2 V^{-1} s^{-1}.[105] Finally solution-processed BHJ OSCs have been tested by mixing compound **DA-10** and $PC_{61}BM$ leading to 3.0 % efficiency and again a high V_{oc} value of 1 V.[106]

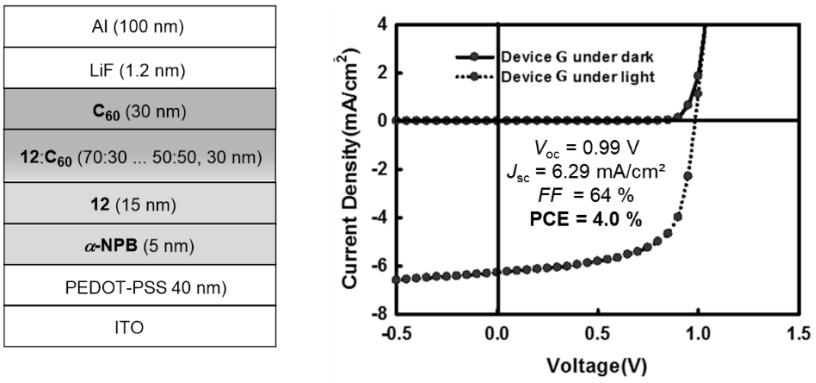

Figure 10: Vacuum-processed BHJ OSC based on **DA-10** and current density *vs* voltage curves under AM 1.5 white light illumination at 100 mW/cm^2. Adapted from ref.105.

Subtle modifications of the structure of **DA-10** were then developed as represented in Scheme 6. Pursuing further the idea of reducing the size of push-pull molecules for OPV, miniaturized systems were synthesized to check their propensity to produce photovoltaic conversion and to use these new platforms for more sophisticated molecules. First, the internal benzene ring of **DA-10** was suppressed affording **DA-11** with a diphenylthienylamine electron-donating block directly end-capped with a DCV unit.[107] The

oxidation peak potential of the first reversible oxidation wave of **DA-11** is shifted toward more positive potential (E_{pa}^1 = 0.78 V *vs* Fc/Fc^+). As expected for a less π-extended system, the absorption maximum in CH_2Cl_2 decreases (λ_{max} = 473 nm). However, bilayer OSCs (ITO/PEDOT-PSS/**DA-11**/C_{60}/Al) were successfully fabricated by spin-casting a $CHCl_3$ solution of **DA-11** leading to a relatively high *PCE* of 1.92 % for such a small molecule. A fused-analogue system **DA-12** based on a thieno[2,3]indole electron-donating block was later reported.[108] This compound exhibits a reversible oxidation wave at highly positive potential E_{pa}^1 = 0.97 V and an irreversible reduction wave at E_{pr}^1 = - 1.72 V. The ICT band of **DA-12** in CH_2Cl_2 decreases down to 452 nm albeit showing high extinction molar coefficients ε of 62 000 M^{-1} cm^{-1}. Thin-films of **DA-12** prepared by vacuum-evaporation showed relatively good hole-transport properties (μ_h = 2.27 × 10^{-5} cm^2 V^{-1} s^{-1}) and were used in bilayer OSCs with C_{60} giving a *PCE* of 1.06 %. This low-molecular weight compound represents the smallest push-pull molecule ever reported with a *PCE* higher than 1 %, further investigations on more extended push-pull systems are still underway.

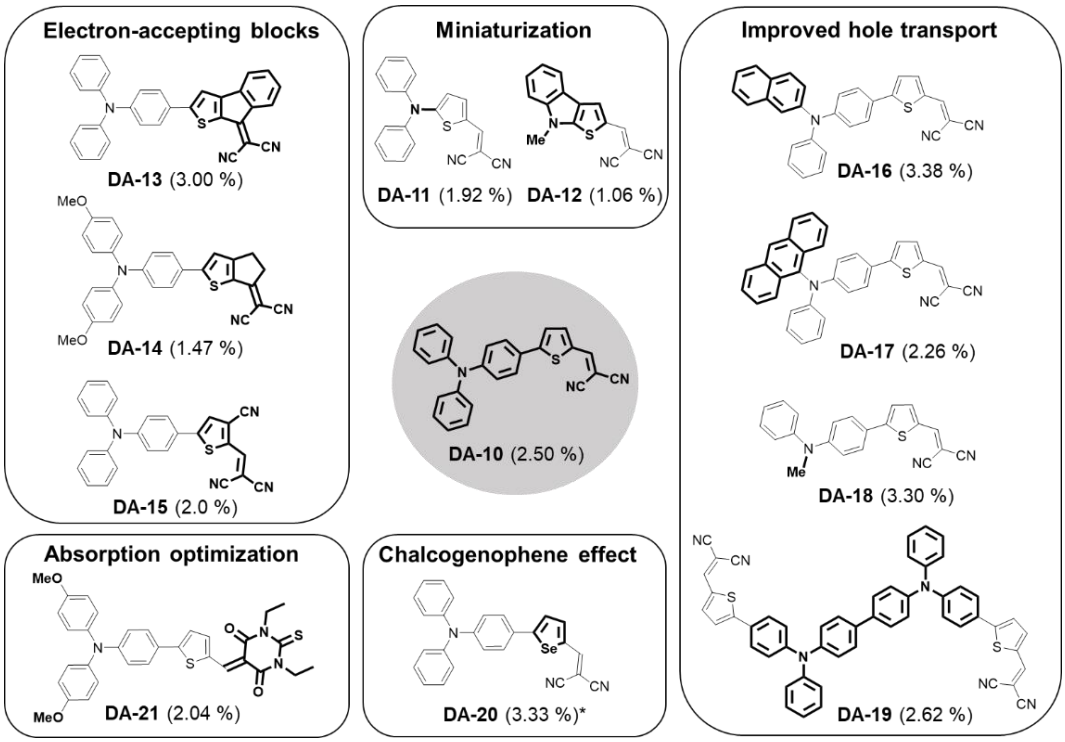

Scheme 6: Examples of structural changes of push-pull donor **DA-10** and *PCE* of related bilayer OSCs with C_{60} (* BHJ OSC with $PC_{61}BM$).

Push-pull molecules with new DCV-based electron-accepting blocks were developed by covalent bridging of the DCV terminal unit of **DA-10** affording compounds **DA-13**[102,103] and **DA-14**,[109] or by introducing an additional nitrile electron-withdrawing in **DA-15**.[104] The best PV performance was obtained with compound **DA-13** where the DCV group has been fused to the thiophene by a phenyl ring. Compared to **DA-10**, the structural change in **DA-13** induces a significant bathochromic shift of the maximum of absorption of the ICT band from 501 nm to 610 nm together with a *ca*. twofold decrease in the molar absorption coefficient ε (Figure 11). The bridging of the DCV unit leads to a negligible decrease in E_{pa}^1 (- 10 mV), but to a large 430 mV positive shift of the reduction wave (E_{pr}^1 = - 1.22 V *vs* Fc/Fc^+). These results show that while the *ortho*-phenylene bridge has a small influence on the HOMO level, it leads to a significant stabilization of the LUMO

level demonstrating the strong electron-withdrawing effect of this new electron-accepting group. The full reversibility of the first reduction wave indicating a stabilization of the reduced state, can be interpreted by the formation of an aromatic cyclopentadienyl radical anion upon reduction. Bilayer OSCs prepared by spin-casting a solution of **DA-13** and subsequent evaporation of C_{60} led to a V_{oc} of 0.97 V, a J_{sc} of 5.32 mA cm^{-2} and a FF of 52 % resulting in a *PCE* of 3.00 %. It is worth mentioning that taking advantage of the complementary optical properties of **DA-10** and **DA-15**, a blend of these compounds was used as donor layer in a bilayer OSC with C_{60} affording a *PCE* of 3.06 %.[104]

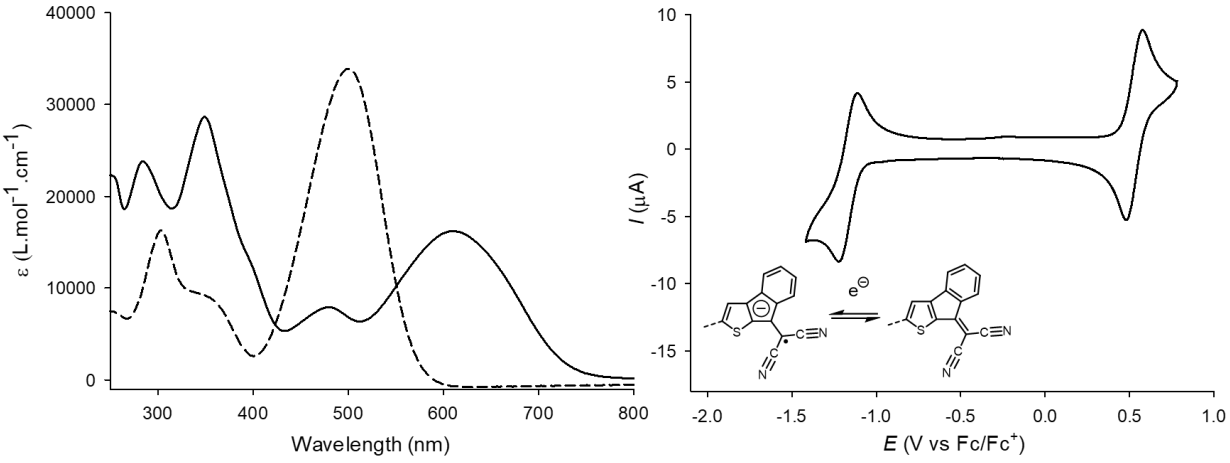

Figure 11: Absorption spectra of **DA-10** (dashed line) and **DA-13** (solid line) in CH_2Cl_2 (Left). CV of **DA-13** 1 mM in 0.1 M Bu_4NPF_6/CH_2Cl_2, Pt working electrode, scan rate 100 mV/s and generation of a cyclopentadienyl radical anion upon electrochemical reduction (Right).

One limitation of small molecules compared to conjugated polymers as donor materials for OPV, is their comparatively weaker hole transport properties. Different molecular engineering approaches have been investigated in our group to tackle this problem. First, one of the external phenyl rings of the TPA of **DA-10** has been replaced

by a π-extended naphthyl platform attached *via* its β position to the nitrogen atom.[110] Compared to reference **DA-10**, this structural modification has nearly no consequences on the electrochemical and optical properties of the resulting molecule **DA-16** (λ_{max} = 500 nm, E_{pa}^1 = 0.58 V and E_{pr}^1 = - 1.63 V *vs* Fc/Fc^+). However, bilayer OSCs with **DA-16** and C_{60} produce a significant increase of *PCE* up to 3.38 % particularly due to a large increase of J_{sc} (7.80 mA cm^{-2}) which can be correlated to a parallel increase of hole mobility μ_h. Indeed a value of μ_h of 5.0 × 10^{-5} cm^2 V^{-1} s^{-1} was measured on thin-films of **DA-16**, a five times higher value than the one measured on **DA-10** probably due to different intermolecular interactions and molecular packing. Pursuing this approach, one outermost phenyl ring of TPA was recently replaced by a 2- or 9-anthryl group.[111] Bilayer OSCs were prepared by spin-casting solutions of these compounds and subsequent evaporation of C_{60}. A higher *PCE* of 2.26 % was measured for the 9-anthryl derivative **DA-17** (*vs* 1.20 % for the 2-anthryl one) due to its better hole transport properties associated to its 3D structure.

Interestingly when one outermost phenyl of **DA-10** is substituted by a methyl group,[112] again the electrochemical and optical properties of the related molecule **DA-18** in solution are nearly identical to those of **DA-10**. However, analysis of single crystals by X-ray diffraction shows a head-to-tail molecular packing for **DA-10**,[103] as very often observed for strongly dipolar push-pull molecules, whereas the crystalline structure of **DA-18** exhibits a completely different co-facial arrangement.[112] Furthermore, the optical bandgaps determined on thin-films of **DA-10** (E_g = 2.00 eV) and **DA-18** differ significantly. In fact, freshly spin-casted thin-films of **DA-18** progressively undergo a red shift with an increase of a new band at 620 nm and an absorption threshold leading to an estimated bandgap of E_g = 1.72 eV. These results show that the replacement of a phenyl by a methyl

substituent strongly affects the molecular organization in the solid state. In addition a fifty-fold increase of μ_h (5.0×10^{-4} cm^2 V^{-1} s^{-1}) was measured for **DA-18** as compared with **DA-10**, which is consistent with a more effective molecular packing. Owing to these good absorption and hole transport properties, PV performance was improved in bilayer OSCs fabricated either by spin-casting or evaporation of **DA-18** leading to *PCE* of 2.92 % and 3.30 %, respectively.[112] A recent theoretical investigation on the effect of the substitution of one outermost phenyl ring of **DA-10** by a naphthyl (**DA-16**) or a methyl (**DA-18**) group confirmed that although the effects of the substituents on the electronic and optical properties are negligible, they have an impact on the molecular packing of the crystalline structure. In particular, the methyl substituent favours a face-to-face π-π packing in the crystal structure improving the transport properties.[113]

It is worth mentioning that a bilayer OSC with the ADA push-pull molecule **DA-19** and C_{60} gave a *PCE* value of 2.62 % and a high J_{sc} value of 8.41 mA cm^{-2}.[114] Although hole-mobility measurements were not performed on thin-films of **DA-19**, it is likely that the preceding PV parameters can be related to good hole transport properties which may be related to the presence of a central TPB unit known to favor hole transport. This dimeric analogue of **DA-10** shows a red shifted ICT band with a maximum at 529 nm, whereas the replacement of a TPA unit by a TPB one leads to two one-electron reversible waves at 0.44 V and 0.63 V *vs* Fc/Fc^+, the negative shift of the first oxidation wave induces a decrease of V_{oc} (0.63 V).

The effect of the nature of the chalcogenophene π-connector in **DA-10** on its electronic properties and PV performance has been investigated.[106] Replacement of furane by thiophene and selenophene leads to a progressive decrease of the optical band gap of the material and to a parallel increase of hole mobility and *PCE*. Thus, a *PCE* of

3.33 % has been obtained for a simple air- and solution-processed BHJ involving the selenophene-based donor **DA-20** and $PC_{61}BM$. On the other hand, structural modulation of the ICT band from 519 nm to 707 nm was achieved in push–pull molecules terminated by a stronger dianisylamino electron-donating block using different π-conjugating spacers and various terminal electron-deficient groups.[115] The use of the dianisylamino group leads to a reversible oxidation wave with lower oxidation potentials values. For instance, the thiobarbituric acid derivative **DA-21** exhibits a E_{pa}^1 value of 0.29 V *vs* Fc/Fc^+. The best bilayer OSC with this TPA-based compound **DA-21** gave a *PCE* of 2.04 % although the V_{oc} value of 0.59 V is relatively low due to the too strong electron-donating character of the dianisylamino group.

More recently, in order to explore the potential of multimers $(DA)_n$ of DA push-pull molecules for OPV, we prepared **Tetra-T** and **Tetra-CPDT**, two tetramers of TPA-based DA push-pull molecules linked by a non-conjugated central pentaerythritol σ-linker (Figure **12**).[116] The two push-pull moieties differ by the presence of a simple thiophene (T) or a more π-extended cyclopentadithiophene (CPDT) as π-spacer between the TPA and a cyanoacrylic ester group. The tetramer based on CPDT exhibits an ICT band at longer wavelength than the thiophene analogue in solution, respectively λ_{max} = 533 nm and 490 nm. While the **Tetra-T** is characterized by one reversible oxidation wave at a E_{pa}^1 value of 0.59 V *vs* Fc/Fc^+ leading to a tetra(radical cation) species, its CPDT counterpart exhibits two reversible oxidation waves peaking at 0.39 V and 0.73 V, respectively assigned to the formation of a stable radical cation and a dication *per* independent push–pull unit. When blended with $PC_{71}BM$ in BHJ OSCs, **Tetra-T** and **Tetra-CPDT** led to the promising *PCE*s of 4.5 %. The V_{oc} value for **Tetra-CPDT** appears slightly lower than that of **Tetra-T** (0.88 V *vs* 0.93 V) in agreement with its lower oxidation potential whereas the J_{sc} value for **Tetra-**

CPDT is slightly increased (12.93 mA cm^{-2} *vs* 12.43 mA cm^{-2}) owing to its better absorption properties. This approach based on multimers of push-pull molecules opens interesting perspectives for the design of new materials for OPV.

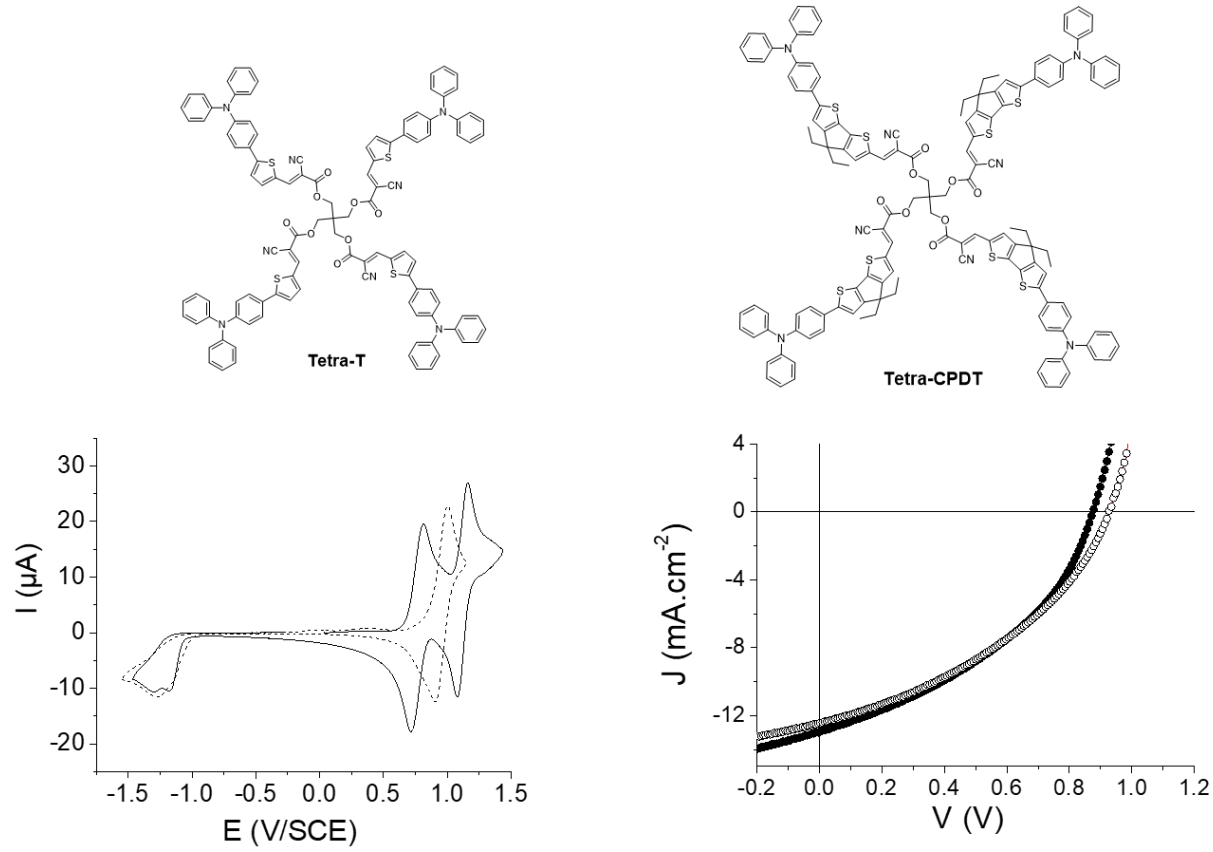

Figure 12: CV of **Tetra-T** (dashed line) and **Tetra-CPDT** (solid line) 0.5 mM in 0.1 M Bu_4NPF_6/CH_2Cl_2, Pt working electrode, scan rate 100 mV/s and current density *vs* voltage curves of BHJ OSCs prepared from **Tetra-T** (white circles) and **Tetra-CPDT** (black circles) under AM 1.5 white light illumination at 100 mW/cm^2. Adapted from reference 116 by permission of *The Royal Society of Chemistry*.

Organic materials where the donor and the acceptor components are covalently linked through a nonconjugated *σ*-connector have been previously explored for the fabrication of single-component organic solar cells (SC-OSCs).[117,118] Compared to BHJ, the photoactive layer of SC-OSCs is expected to be less subjected to morphology evolution. In addition, owing to the close proximity of the donor and acceptor components, exciton dissociation on the same molecule may avoid the limiting step of exciton diffusion

associated with organic semiconductors. However PV performance of SC-OSCs are still lower than those of BHJ OSCs and most materials evaluated in SC-OSCs led to *PCE* values often much below 0.5 %. However SC-OSCs using discrete molecules such as a dithiafulvalene-functionalized diketopyrrolopyrrole-C_{60} dyad[119] and a triad based on an oligothiophene-fullerene conjugate[120] have recently led to encouraging *PCEs* of 2.2 % and 2.4 %, respectively.

In this context, our group has recently reported the synthesis of **TPA-T-C_{60}**, a TPA-based DA push-pull−σ−C_{60} dyad.[121] The latter shows a broad ICT band at 478 nm characteristic of the push−pull moiety and the presence of specific absorption bands at 259 and 327 nm, together with a discernible band at 431 nm characteristic of the fullerene unit (Figure 13). Also the CV of **TPA-T-C_{60}** exhibits both the electrochemical signatures of the push-pull moiety and $PC_{61}BM$. Thus, the reversible oxidation wave at E_{pa}^1 = 0.57 V and the irreversible reduction wave at E_{pr}^3 = - 1.69 V *vs* Fc/Fc^+ are associated to the formation of the radical cation and radical anion of the push-pull moiety while the two first reversible reduction waves at E_{pr}^1 = - 1.15 V and E_{pr}^2 = - 1.53 V *vs* Fc/Fc^+ correspond to the stable radical anion and dianion of the fullerene unit (Figure 13). Spectroelectrochemical analysis revealed the optical signatures of the radical cation of the push-pull moiety and the radical anion of the fullerene unit. The former one mainly exhibits two strong broad absorption bands peaking at 610 and 1033 nm whereas the latter one is characterized by a weak band at 1030 nm. SCLC measurements gave an electron mobility of $\mu_e = 4.3 \times 10^{-4}$ cm^2 V^{-1} s^{-1}, *ca*. 50 times higher than the hole mobility. SC-OSCs with the following structure ITO/PEDOT-PSS/**TPA-T-C_{60}**/Ca/Al were characterized by an open-circuit voltage V_{oc} of 0.73 V, a short-circuit current density of 2.1 mA cm^{-2}, a poor fill factor *FF* of 29 %, overall resulting in a *PCE* of 0.4 %. Transient

absorption spectroscopy time delayed collection field experiments confirmed that photoexcitation of a thin-film of **TPA-T-C$_{60}$** led to an ultrafast and efficient charge generation and showed the presence of pure fullerene domains. However, the fast recombination competes with the extraction of separated charges hence giving rise to SC-OSCs with relatively poor PV performance. Nevertheless, these results reveal that charge percolation is possible in these devices and that new molecular dyads with self-assembly properties for optimized nanophase separation could be of interest.

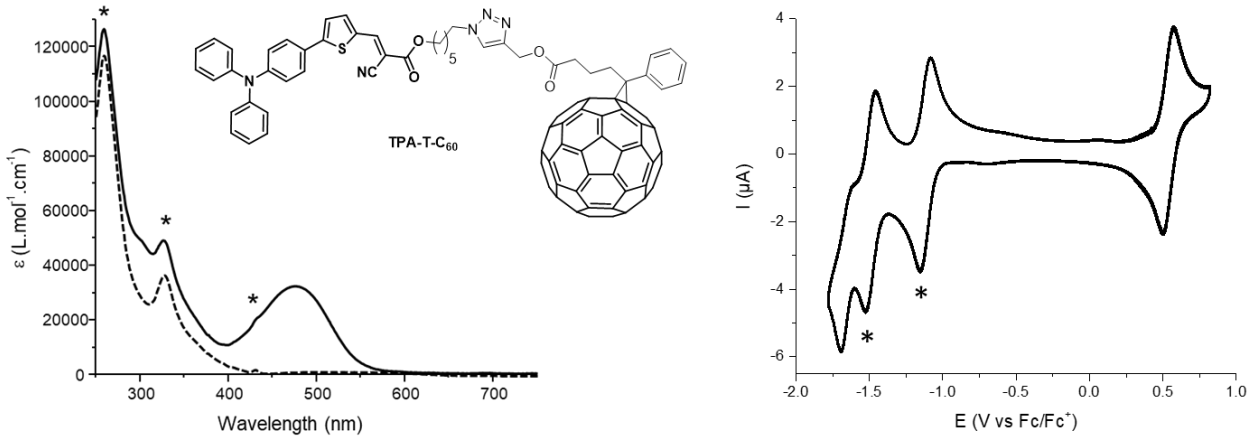

Figure 13: Structure of **TPA-T-C$_{60}$**, UV-vis spectra of **TPA-T-C$_{60}$** (solid line) and $PC_{61}BM$ (dashed line) in CH_2Cl_2 and CV of **TPA-T-C$_{60}$** in 0.1 M Bu_4NPF_6/CH_2Cl_2, Pt working electrode, scan rate 100 mV/s. The stars highlight the electrochemical and optical signatures of the fullerene moiety of **TPA-T-C$_{60}$**. Adapted from ref. 121.

4. Conclusion

Owing to their relative ease of synthesis and their adapted electronic properties that can be finely tuned by known synthetic reactions, triphenylamine and its derivatives represent excellent building blocks for the preparation of electroactive materials for opto-electronic devices. A number of TPA-based amorphous materials have been used as hole

transporting/injection layer in OLEDs, field-effect transistors or OSCs. On the other hand, push-pull molecules based on TPA constitute outstanding photoactive donor materials for OSCs. This article has given an overview of this important class of materials highlighting the relation between their structure and their optical and electrochemical properties and additionally their photovoltaic performances. In particular, simple and cost-effective linear TPA-based DA push-pull molecules have led to solution or vacuum-processed single junction OSCs showing power conversion efficiencies as high as 8%. Moreover, very recent works from the literature have demonstrated that simple DA push-pull systems can be implemented in tandem or triple junction OSCs with record efficiencies up to 15 % hence stimulating further research. As illustrated in this review, the group of Angers has investigated a large number of small, efficient and scalable push-pull molecules for OPV following different molecular engineering approaches. While new small push-pull molecules are still under investigation, the recent development of easily accessible multimers of push-pull molecules could represent an interesting perspective for OPV.

From an electrochemistry and polymer science viewpoint, the propensity of some TPA derivatives to lead to unstable radical cations upon (electro)chemical oxidation and subsequent couplings, has been discussed and particularly exploited by the group of Stuttgart for the synthesis of crosslinked electroactive polymer films. As main methods in-situ spectroelectrochemistry of solutions and films and cyclic voltammetry coupled with *in situ* conductance measurements have been applied to study mechanisms and identify the generated redox species.

Our strategy of chemically synthesizing tailor-made polymers and block copolymers, solution processing them into film architectures and subsequently inducing

the crosslinking reaction or post-polymerization is particularly relevant for applications in organic electronics and nanotechnology applications.

In the case of a PSTPA, well resolved conductivity regimes could be identified which were explained by mixed valence conductivity, as is characteristic for redox polymers. Especially the possibility to chemically synthesize tailor-made block copolymers from PSTPA and a soft-degradable polymer block such as poly(lactide) are highly attractive for the preparation of electroactive nanoporous templates.

Attaching TPA further to conjugated regioregular polythiophene backbones yields conjugated redox polymers which after electrochemical crosslinking lead to stable highly conducting polymer films. Learning from electrochemistry we have transferred the crosslinking reaction to occur in an analogous way with chemical dopants as proven by four point probe measurements yielding conductivities as high as 8 S/cm. Highly conducting polymer films which are additionally reasonably transparent will be further exploited as hole transport layers in solar cells and future alternative applications will include thermoelectric devices.

Acknowledgments

We thank Prof. J. Heinze, Prof. U. Steiner, Prof. M. Hillmyer, Dr. O. Yurchenko, Dr. E.J.W. Crossland, P. Reinold and K. Bruchlos for their highly valuable contributions to the respective studies. Financial support was given by the German Science Foundation within an Emmy Noether Grant. We thank all the PhD and postdoctoral students involved in the OPV projects. Colleagues from MOLTECH-Anjou, Dr. A. Cravino, Prof. P. Leriche, Pr. P. Frère, Dr. F. Gohier, Dr. O. Segut, Dr. O. Alévêque, Dr. J-C. Bernède and Dr. L. Sanguinet are acknowledged for their contributions as well as collaborators Dr. D. Tondelier from Ecole Polytechnique, Palaiseau (France), Dr. B. Geffroy from CEA Saclay (France) and Prof. F. Laquai and Dr. J. Gorenflot from King Abdullah University of Science and Technology (Saudi Arabia).

References

1. Shirota Y, *J Mater Chem* **10**:1-25 (2000)

2. Degli Esposti A, Fattori V, Sabatini C, Casalbore-Miceli G, Marconi G, *Phys Chem Chem Phys* **7**:3738–3743 (2005)

3. Shirota Y, Kageyama H, *Chem Rev* **107**:953-1010 (2007)

4. Cias P, Slugovc C, Gescheidt G, *J Phys Chem A* **115**:14519-14525 (2011)

5. Thelakkat M, *Macromol Mater Eng* **287**:442-461 (2002)

6. Rybakiewicz R, Zagorska M, Pron A, *Chem Pap* **71**:243-268 (2017)

7. Bellmann E, Shaheen SE, Thayumanavan S, et al., *Chem Mater* **10**:1668-1676 (1998)

8. Kwak J, Bae WK, Zorn M, et al., *Adv Mater* **21**:5022-5026 (2009)

9. Chou MY, Leung MK, Su YO, et al., *Chem Mater* **16**:654-661 (2004)

10. Roncali J, Leriche P, Blanchard P, *Adv Mater* **26**:3821-3838 (2014)

11. Malytskyi V, Simon J-J, Patrone L, Raimundo J-M, *RSC Adv* **5**:354-397 (2015)

12. Wang J, Liu K, Ma L, Zhan X, *Chem Rev* **116**:14675-14725 (2016)

13. Ning Z, Tian H, *Chem Commun* **0**:5483–5495 (2009)

14. Agarwala P, Kabra D, *J Mater Chem A* **5**:1348-1373 (2017)

15. Su C, Yang F, Ji L, Xu L, Zhang C, *J Mater Chem A* **2**:20083-20088 (2014)

16. Zhuang H, Zhou Q, Zhang Q, et al., *J Mater Chem C* **3**:416-422 (2015)

17. Wu J-H, Liou G-S, *ACS Appl Mater Interfaces* **7**:15988-15994 (2015)

18. Paine AJ, *J Am Chem Soc* **109**:1496-1502 (1987)

19. Manifar T, Rohani S, *Can J Chem Eng* **82**:323-334 (2004)

20. Driver MS, Hartwig JF, *J Am Chem Soc* **118**:7217-7218 (1996)

21. Wolfe, John P, Wagaw S, Buchwald SL, *J Am Chem Soc* **118**:7215-7216 (1996)

22. Hatakeyama T, Imayoshi R, Yoshimoto Y, et al., *J Am Chem Soc* **134**:20262-20265 (2012)

23. Munshi MU, Berden G, Martens J, Oomens J, *Phys Chem Chem Phys* **19**:19881-19889 (2017)

24. Reva I, Lapinski L, Chattopadhyay N, Fausto R, *Phys Chem Chem Phys* **5**:3844-3850 (2003)

25. Wang BC, Liao HR, Chang JC, Chen L, Yeh JT, *J Lumin* **124**:333-342 (2007)

26. Wu J, Wilson BA, Smith Jr. DW, Nielsen SO, *J Mater Chem C* **2**:2591-2599 (2014)

27. Hagberg DP, Marinado T, Karlsson KM, et al., *J Org Chem* **72**:9550-9556 (2007)

28. Pan JH, Chiu HL, Chen L, Wang BC, *Comput Mater Sci* **38**:105-112 (2006)

29. Bender TP, Graham JF, Duff JM, *Chem Mater* **13**:4105-4111 (2001)

30. Seo ET, Nelson RF, Fritsch JM, Marcoux LS, Leedy DW, Adams RN, *J Am Chem Soc* **88**:3498-3503 (1966)

31. Nelson RF, Adams RN, *J Am Chem Soc* **90**:3925-3930 (1968)

32. Creason SC, Wheeler J, Nelson RF, *J Org Chem* **37**:4440-4446 (1972)

33. Nelson RF, Philp RH, *J Phys Chem* **83**:713-716 (1979)

34. Yurchenko O, Freytag D, Zur Borg L, Zentel R, Heinze J, Ludwigs S, *J Phys Chem B* **116**:30-39 (2012)

35. Sreenath K, Suneesh CV, Ratheesh Kumar VK, Gopidas KR, *J Org Chem* **73**:3245-3251 (2008)

36. Crossland EJW, Cunha P, Scroggins S, et al., *ACS Nano* **4**:962-966 (2010)

37. Heinze J, Frontana-Uribe BA, Ludwigs S, *Chem Rev* **110**:4724-4771 (2010)

38. Barth M, Guilerez S, Bidan G, Bras G, Lapkowski M, *Electrochim Acta* **45**:4409-4417 (2000)

39. Smie A, Synowczyk A, Heinze J, et al., *J Electroanal Chem* **452**:87-95 (1998)

40. Dapperheld S, Steckhan E, Brinkhaus K-HG, Esch T, *Chem Ber* **124**:2557-2567 (1991)

41. Bäuerle P, *Adv Mater* **4**:102-107 (1992)

42. Engelmann G, Kossmehl G, Heinze J, Tschuncky P, Jugelt W, Welzel H-P, *J Chem Soc, Perkin Trans 2* **0**:169-176 (1998)

43. Reynolds R, Line LL, Nelson RF, *J Am Chem Soc* **96**:1087–1092 (1974)

44. Yurchenko O, Heinze J, Ludwigs S, *ChemPhysChem* **11**:1637-1640 (2010)

45. Choi K, Yoo SJ, Sung Y-E, Zentel R, *Chem Mater* **18**:5823-5825 (2006)

46. Sommer M, Lindner SM, Thelakkat M, *Adv Funct Mater* **17**:1493-1500 (2007)

47. Kang HA, Bronstein HE, Swager TM, *Macromolecules* **41**:5540-5547 (2008)

48. Jiang G, Huang C, Baba A, Advincula R, *Macromol React Eng* **6**:153-159 (2012)

49. Torrance JB, *Acc Chem Res* **12**:79-86 (1979)

50. Chidsey CED, Murray RW, *J Phys Chem* **90**:1479-1484 (1986)

51. John H, Bauer R, Espindola P, Sonar P, Heinze J, Müllen K, *Angew Chemie - Int Ed* **44**:2447-2451 (2005)

52. Crossland EJW, Nedelcu M, Ducati C, et al., *Nano Lett* **9**:2813-2819 (2009)

53. Crossland EJW, Kamperman M, Nedelcu M, et al., *Nano Lett* **9**:2807-2812 (2009)

54. Zalusky AS, Olayo-Valles R, Wolf JH, Hillmyer MA, *J Am Chem Soc* **124**:12761-12773 (2002)

55. Cummins C, Mokarian-Tabari P, Holmes JD, Morris MA, *J Appl Polym Sci* **131**:40798 (2014)

56. Whiting GL, Snaith HJ, Khodabakhsh S, et al., *Nano Lett* **6**:573-578 (2006)

57. Reinold P, Bruchlos K, Ludwigs S, *Polym Chem* **8**:7351-7359 (2017)

58. Yamamoto J, Furukawa Y, *J Phys Chem B* **119**:4788-4794 (2015)

59. Su C, Ye Y, Xu L, Zhang C, *J Mater Chem* **22**:22658–22662 (2012)

60. Roquet S, Cravino A, Leriche P, Alévêque O, Frère P, Roncali J, *J Am Chem Soc* **128**:3459-3466 (2006)

61. Cravino A, Leriche P, Alévêque O, Roquet S, Roncali J, *Adv Mater* **18**:3033-3037 (2006)

62. Leriche P, Frère P, Cravino A, Alévêque O, Roncali J, *J Org Chem* **72**:8332-8336 (2007)

63. Ripaud E, Rousseau T, Leriche P, Roncali J, *Adv Energy Mater* **1**:540-545 (2011)

64. Bernède JC, Cattin L, Makha M, et al., *Sol Energy Mater Sol Cells* **110**:107-114 (2013)

65. Min J, Luponosov YN, Baran D, et al., *J Mater Chem A* **2**:16135-16147 (2014)

66. Min J, Luponosov YN, Gerl A, et al., *Adv Energy Mater* **4**:1301234 (2014)

67. Shang H, Fan H, Liu Y, Hu W, Li Y, Zhan X, *Adv Mater* **23**:1554-1557 (2011)

68. Cho N, Paek S, Jeon J, Song K, Sharma GD, Ko J, *J Mater Chem A* **2**:12368 (2014)

69. Aytun T, Santos PJ, Bruns CJ, et al., *J Phys Chem C* **120**:3602-3611 (2016)

70. Paek S, Cho N, Cho S, Lee JK, Ko J, *Org Lett* **14**:6326-6329 (2012)

71. Paek S, Choi H, Sim J, Song K, Lee JK, Ko J, *J Phys Chem C* **118**:27193-27200 (2014)

72. Lim K, Lee SY, Song K, et al., *J Mater Chem C* **2**:8412-8422 (2014)

73. Fang Z, Teo TL, Cai L, Lal YH, Samoc A, Samoc M, *Org Lett* **11**:1-4 (2009)

74. Fang Z, Chellappan V, Webster RD, et al., *J Mater Chem* **22**:15397 (2012)

75. Wang X, Zheng X, Wang X, et al., *J Am Chem Soc* **135**:14912-14915 (2013)

76. Zhang J, Wu G, He C, Deng D, Li Y, *J Mater Chem* **21**:3768 (2011)

77. Lin Y, Cheng P, Liu Y, et al., *Sol Energy Mater Sol Cells* **99**:301-307 (2012)

78. Cheng P, Shi Q, Lin Y, Li Y, Zhan X, *Org Electron* **14**:599-606 (2013)

79. Zeng S, Yin L, Ji C, et al., *Chem Commun* **48**:10627 (2012)

80. Wang L, Yin L, Ji C, Li Y, *Dye Pigm* **118**:37-44 (2015)

81. Chi LC, Chen HF, Hung WY, et al., *Sol Energy Mater Sol Cells* **109**:33-39 (2013)

82. Wang S, Hall L, Diev V V., et al., *Chem Mater* **23**:4789-4798 (2011)

83. Wei G, Xiao X, Wang S, et al., *ACS Nano* **6**:972-978 (2012)

84. Kumar CV, Cabau L, Koukaras EN, Sharma GD, Palomares E, *Org Electron* **26**:36-47

(2015)

85. Leliège A, Blanchard P, Rousseau T, Roncali J, *Org Lett* **13**:3098-3101 (2011)

86. Wu X, Wu J, Liu Y, Jen AK, *J Am Chem Soc* **121**:2391-2392 (1999)

87. Kato S, Diederich F, *Chem Commun* **46**:1994 (2010)

88. Po R, Roncali J, *J Mater Chem C* **4**:3677-3685 (2016)

89. Jeux V, Segut O, Demeter D, et al., *Dye Pigm* **113**:402-408 (2015)

90. Faurie A, Grolleau J, Gohier F, Allain M, Legoupy S, Frère P, *Eur J Org Chem* **2017**:2707-2714 (2017)

91. Xia PF, Feng XJ, Lu J, et al., *Adv Mater* **20**:4810-4815 (2008)

92. Ko HM, Choi H, Paek S, et al., *J Mater Chem* **21**:7248 (2011)

93. Lin H-W, Lin L-Y, Chen Y-H, et al., *Chem Commun* **47**:7872 (2011)

94. Kozlov O V., Luponosov YN, Solodukhin AN, et al., *Org Electron* **53**:185-190 (2018)

95. Chiu S-W, Lin L-Y, Lin H-W, et al., *Chem Commun* **48**:1857-1859 (2012)

96. Lin LY, Chen YH, Huang ZY, et al., *J Am Chem Soc* **133**:15822-15825 (2011)

97. Chen YH, Lin LY, Lu CW, et al., *J Am Chem Soc* **134**:13616-13623 (2012)

98. Shim HS, Moon CK, Kim J, et al., *ACS Appl Mater Interfaces* **8**:1214-1219 (2016)

99. Che X, Xiao X, Zimmerman JD, Fan D, Forrest SR, *Adv Energy Mater* **4**:1400568 (2014)

100. Che X, Li Y, Qu Y, Forrest SR, *Nat Energy* **3**:422-427 (2018)

101. Mishra A, Wetzel C, Singhal R, Sharma GD, *J Phys Chem C* **112**:11262-11269 (2018)

102. Leliège A, Régent C-H Le, Allain M, Blanchard P, Roncali J, *Chem Commun* **48**:8907–8909 (2012)

103. Leliège A, Grolleau J, Allain M, et al., *Chem Eur J* **19**:9948-9960 (2013)

104. Grolleau J, Gohier F, Allain M, Legoupy S, Cabanetos C, Frère P, *Org Electron* **42**:322-328 (2017)

105. Choi JW, Kim C-H, Pison J, et al., *RSC Adv* **4**:5236-5242 (2014)

106. Labrunie A, Jiang Y, Baert F, et al., *RSC Adv* **5**:102550-102554 (2015)

107. Jeux V, Demeter D, Leriche P, Roncali J, *RSC Adv* **3**:5811-5814 (2013)

108. Baert F, Cabanetos C, Allain M, Silvestre V, Leriche P, Blanchard P, *Org Lett* **18**:1582-1585 (2016)

109. Demeter D, Jeux V, Leriche P, et al., *Adv Funct Mater* **23**:4854-4861 (2013)

110. Mohamed S, Demeter D, Laffitte JA, Blanchard P, Roncali J, *Sci Rep* **5**:9031 (2015)

111. Jiang Y, Cabanetos C, Jungsuttiwong S, Alberga D, Adamo C, Roncali J, *ChemistrySelect* **2**:6296-6303 (2017)

112. Jiang Y, Cabanetos C, Allain M, Liu P, Roncali J, *J Mater Chem C* **3**:5145-5151 (2015)

113. Alberga D, Ciofini I, Mangiatordi GF, et al., *Chem Mater* **29**:273-281 (2017)

114. Diac A, Demeter D, Jungsuttiwong S, Grosu I, Roncali J, *Tetrahedron Lett* **56**:4607-4612 (2015)

115. Jeux V, Segut O, Demeter D, Alévêque O, Leriche P, Roncali J, *Chempluschem* **80**:697-703 (2015)

116. Labrunie A, Josse P, Dabos-Seignon S, Blanchard P, Cabanetos C, *Sustain Energy Fuels*

1:1921-1927 (2017)

117. Segura JL, Martín N, Guldi DM, *Chem Soc Rev* **34**:31-47 (2005)

118. Roncali J, *Adv Energy Mater* **1**:147-160 (2011)

119. Narayanaswamy K, Venkateswararao A, Nagarjuna P, et al., *Angew Chemie - Int Ed* **55**:12334-12337 (2016)

120. Nguyen TL, Lee TH, Gautam B, et al., *Adv Funct Mater* **27**:1702474 (2017)

121. Labrunie A, Gorenflot J, Babics M, et al., *Chem Mater* **30**:3474-3485 (2018)

Table 1: HOMO, LUMO energies, ionization potentials (I_p) for different tri-*para*-substituted TPA derivatives obtained from DFT calculations. Data extracted from reference 4.

R	HOMO energy (eV)	LUMO energy (eV)	ΔE(H-L) (eV)	I_p (eV)
-H	-5.188	-0.720	4.468	6.608
$-NH_2$	-4.247	-0.451	3.796	5.569
$-OCH_3$	-4.649	-0.645	4.004	5.961
$-CH_3$	-4.925	-0.629	4.296	6.265
-Cl	-5.572	-1.290	4.282	6.891
-CN	-6.420	-2.345	4.075	7.696
$-NO_2$	-6.740	-3.228	3.512	8.036

Table 2: Characteristic absorption bands and potentials for TPA, TPB and *p*-TTA and associated redox species upon electrochemical oxidation.[34]

	λ_{max} [nm]			Electrochemical potential	
Species	**Neutral**	**Radical cation**	**Dication**	$E^{p}_{ox,I}$ [V vs $Fc\|Fc^+$]	$E^{1/2}_{ox,I}$ [V vs $Fc\|Fc^+$]
TPA	302	340; 562; 658	-	0.69	-
TPB	352	484	722, 450	0.35	0.25
p-TTA	365	365; 589; 675	-	0.45	0.31